The Organization of Endoplasmic Reticulum Export Complexes

Sergei I. Bannykh, Tony Rowe, and William E. Balch

The Scripps Research Institute, Departments of Cell and Molecular Biology, 10550 North Torrey Pines Road, La Jolla, California 92130

Abstract. Export of cargo from the ER occurs through the formation of 60–70-nm COPII-coated vesicular carriers. We have applied serial-thin sectioning and stereology to quantitatively characterize the three-dimensional organization of ER export sites in vivo and in vitro. We find that ER buds in vivo are nonrandomly distributed, being concentrated in regional foci we refer to as export complexes. The basic organization of an export complex can be divided into an active COPII-containing budding zone on a single ER cisterna, which is adjacent to budding zones found on distantly connected ER cisternae. These budding foci surround and face a central cluster of morphologically independent vesicular-tubular elements that contain COPI coats involved in retrograde transport. Vesicles within these export complexes contain concentrated cargo molecules. The structure of vesicular-tubular clusters in export complexes is particularly striking in replicas generated using a quick-freeze, deep-etch approach to visualize for the first time their three-dimensional organization and cargo composition. We conclude that budding from the ER through recruitment of COPII is confined to highly specialized export complexes that topologically restrict anterograde transport to regional foci to facilitate efficient coupling to retrograde recycling by COPI.

EXPORT of protein from the ER is the first step in the vectorial movement of cargo through compartments of the secretory pathway of eukaryotic cells. Pioneering studies by Palade (1975) established that the site of exit from the RER in pancreatic acinar cells is through transitional elements, a region of partly rough, partly smooth tubular ER juxtaposed to the *cis* face of the Golgi stack. Morphologically, ER-derived vesicles are 60–70 nm in diameter and contain an electron-dense coat when viewed using transmission electron microscopy (Ziegel and Dalton, 1962). This characteristic coat contains COPII components that are assembled in response to the activation of the Sar1 GTPase, a machinery now recognized to be evolutionarily conserved in yeast and mammalian cells (for review see Barlowe, 1995).

While the formation of ER to Golgi carrier vesicles in secretory tissues is largely confined to the transitional region facing the juxtanuclear Golgi apparatus (Palade, 1975), studies in other cell lines have shown that export from the ER can originate from multiple sites that appear randomly distributed throughout the cytoplasm and, in most instances, distant from the Golgi complex. The relationship of these peripheral sites to the transitional region found in secretory cells is unknown, although they are now recognized to consist of clusters of small vesicles and tubular elements (Saraste and Kuismanen, 1984; Schweizer et al., 1990; Saraste and Svensson, 1991; Lotti et al., 1992) referred to as vesicular tubular clusters (VTCs)[1] (Balch et al., 1994). While VTCs are readily detectable at 37°C in vivo (Saraste and Kuismanen, 1984; Saraste and Svensson, 1991) and at 32°C in vitro (Plutner et al., 1992; Pind et al., 1994*a*), visualization of these structures can be markedly enhanced by incubation of cells at reduced temperature (15°-16°C) (Saraste and Kuismanen, 1984), presumably due to a rate-limiting step in membrane flow through these intermediates. Elements of VTCs lack luminal continuity with the ER (Saraste and Svensson, 1991; Balch et al., 1994; Connolly et al., 1994), although tubular extensions of ER into these structures have been observed (Stinchcombe et al., 1995), particularly in cells infected with certain viruses (Tooze et al., 1984; Krijnse-Locker et al., 1994), reinforcing their close relationship to ER export.

VTCs are dynamic structures with varied morphology in different cell types. In the past, VTCs have been suggested to be the site of O-glycosylation (Tooze et al., 1988), acylation (Rizzolo et al., 1985), and generation of the mannose-6-phosphate signal for lysosomal protein targeting (Pelham, 1988). Several endogenous proteins serve as useful markers for VTCs. These include the small GTPase Rab2 (Chavrier et al., 1990), the transmembrane protein p58 in rat cells or its human homologue p53 (Schweizer et al., 1988; Saraste and Svensson, 1991), which actively cycle between the ER and VTCs, and the COPI subunit β-COP (Oprins et al., 1993; Pepperkok et al., 1993; Pind et al.,

Address all correspondence to William E. Balch, The Scripps Research Institute, Departments of Cell and Molecular Biology, 10550 N. Torrey Pines Road, La Jolla, CA 92130. Tel.: (619) 554-2310. Fax: (619) 554-6253. e-mail: webalch@scripps.edu.

1. *Abbreviations used in this paper*: CGN, *cis*-Golgi network; GA, glutaraldehyde; NRK, normal rat kidney; RBL, rat basophilic leukemia; rt, room temperature; TEM, transmission EM; VSV-G, vesicular stomatitis virus glycoprotein; VTC, vesicular tubular cluster.

1994*a*; Aridor et al., 1995). VTCs play a pivotal role in the segregation of anterograde and retrograde transported proteins (Aridor et al., 1995; Tang et al., 1995). Segregation is believed to involve the COPI coat complex whose assembly is driven through activation of the ARF1 GTPase (Aridor et al., 1995; Letourneur et al., 1995).

While VTC composition and function have been described qualitatively through use of immunofluorescence (Lotti et al., 1992; Aridor et al., 1995; Lippincott-Schwartz et al., 1995) and immunoperoxidase (Connolly et al., 1994; Stinchcombe et al., 1995) approaches, the topology of ER budding sites and, in particular, their relationship to VTCs have not been studied quantitatively at high resolution. In the present paper, we use both transmission TEM and immunoelectron microscopy in conjunction with quick-freeze, deep-etch methods to reconstruct these relationships morphometrically and to confirm that cargo is concentrated during vesicle budding. We find that almost all ER buds detected in the cell were concentrated in regional foci facing VTCs, which had a characteristic diameter and vesicular-tubular composition. As such, the topological organization of buds and VTCs defines a morphological unit of function, which we refer to as export complexes. We conclude that budding from the ER is not evenly distributed along the membrane, but is confined to specific export sites. These are highly enriched in COPII and COPI transport components and are likely to promote the coupling of anterograde and retrograde transport.

Materials and Methods

Materials

A polyclonal antibody specific for yeast Sec23p that cross-reacts with a mammalian homologue (Orci et al., 1991) was obtained from R. Schekman (University of California, Berkeley). Affinity-purified antibodies specific for yeast Sec13p that cross-reacts with a mammalian homologue (Shaywitz et al., 1995) were a generous gift of C. Kaiser (Massachusetts Institute of Technology, Cambridge, MA). A hybridoma cell line expressing an mAb specific for the carboxyl terminus of vesicular stomatitis virus glycoprotein (VSV-G) (P5D4) was provided by T. Kreis (University of Geneva, Switzerland) (Kreis, 1986). Secondary antibodies were obtained from the following sources: Texas red–conjugated goat anti–mouse IgG from Zymed Laboratories (South San Francisco, CA), 6 nm gold–conjugated goat anti–mouse and anti–rabbit antibodies from Jackson Immunoresearch Laboratories (West Groven, PA), and 10 nm gold–conjugated goat anti–mouse antibodies from Amersham Corp. (Arlington Heights, IL). Sar1 wild type and the H79G and T39N mutant proteins were prepared as described (Aridor et al., 1995). All other reagents, except where indicated, were obtained from Sigma Chemical Co. (St. Louis, MO).

Cells and Virus

Normal rat kidney (NRK) and rat basophilic leukemia (RBL) cells (RBL-2H3) were maintained in monolayer culture in α-MEM supplemented with penicillin, streptomycin, and 7% (NRK) or 16% (RBL) FBS (Gemini Bioproducts, Calabasas, CA) as described (Plutner et al., 1992). Ts045-VSV (Lafay, 1974) was propagated in BHK-21 cells as described (Beckers et al., 1987). Cells were infected with ts045-VSV at a multiplicity of 10–20 plaque-forming units per cell as described (Davidson and Balch, 1993).

Epon Embedding and Serial Sectioning

Cells were fixed in 2.5% glutaraldehyde (GA) in PBS for 1 h at room temperature (rt), scraped in GA, and pelleted at 15,000 *g* in a microcentrifuge for 10 min. The tight pellet was washed in veronal-acetate buffer (pH 6.0) and stained in 1% buffered OsO_4 for 1 h at rt. After washing in veronal-acetate buffer, pellets were stained en bloc with 2% uranyl acetate in veronal-acetate buffer, dehydrated in alcohol and acetone, and embedded in Epon 812 (Electron Microscopy, Sciences, Fort Washington, PA). For serial sectioning, the cell pellet was cut with a glass knife followed by trimming of the resulting block to obtain an ~40 ×300 μm pyramid. A ribbon of 25–35 consecutive sections of 65 nm in thickness was cut with a diamond knife on Reichert ultramicrotome 2E and transferred to a single 2 × 1.5 mm slot grid (Electron Microscopy Sciences) precoated with a Formvar/carbon film. Sections were counterstained with a saturated solution of uranyl acetate in methanol for 10 min at rt and Reynold's lead citrate for 10 min. Budding structures on the ER and VTCs were followed in consecutive sections, and images were overlaid to reconstruct continuity between structures.

Transmission EM and Morphometry

Stereological Parameters. An estimation of the mean volume of the cells was performed by two independent methods (Baddeley et al., 1985; Griffiths et al., 1989). In the first case, RBL cells were grown on glass coverslips. Cells were fixed with 2.5% GA in PBS, pH 7.4, overnight. The cells were then viewed and photographed under phase contrast with an Axiophot (Zeiss, Oberkochen, Germany) with a ×20 objective lens. The images were enlarged photographically 10 times, and the mean surface of the cell projection was determined by the point-counting method (Weibel, 1979) using a 5-mm square lattice grid. Approximately 10,000 RBL cells were used for the estimation of the mean surface of the cell projection onto a planar surface. The cells on coverslips were stained and embedded in Epon as described above. After polymerization, the coverslips were detached from the resin by plunging into liquid nitrogen. Thin-strips of embedded cells in resin were then combined face to face and reembedded on top of an Epon block to produce "vertical" sections (Griffiths et al., 1984). Images of cells were taken with a transmission electron microscope (1200EX; JEOL USA, Peabody, MA) and photoenlarged (×3,500 total magnification), and the mean height of ~250 cells in a monolayer was measured by the point-counting method (Weibel, 1979). The mean cell volume (*V*c.r.) was then determined according to formula:

$$Vc.r. = Sc.p. \times Hc., \quad (1)$$

where *S*c.p. is the mean surface of the cell projection (determined by the phase-contrast light microscopy), and *H*c. is the mean height of the cell (determined by TEM).

For estimation of the mean cell volume using the second method, NRK and RBL cells were grown on 35-mm tissue-culture dishes (Costar Corp., Cambridge, MA), fixed in the dish in 2.5% GA in PBS for 1 h at rt, and processed for TEM as described above. The cell pellet was cut with a diamond knife on a Reichert ultramicrotome 2E. 60–65-nm sections were counterstained as described above. Approximately 1,200 RBL and 800 NRK cells were randomly chosen and photoenlarged to a magnification of 14,000. The mean surface of the cells on sections were measured by the point-counting method (Weibel, 1979). The mean cell volume was found according to formula (Weibel and Gomez, 1962):

$$Vc.r. = 1.4\,(Sc.s.)^{3/2}, \quad (2)$$

where *S*c.s. is the mean cell surface on thin-section. The surface to volume ratio was found according to formula:

$$Sv. = \Sigma I/\Sigma P \times d, \quad (3)$$

where *I* is the number of intersections on a grid, *P* is the number of points on the grid, and *d* is the distance between the points (Weibel, 1979). Both procedures yielded nearly identical results for RBL cells. The values obtained from the second procedure are reported in Table I.

The stereological parameters of nuclei, ER, and Golgi apparatus were determined using the same sections. Randomly taken cell contours were enlarged to a total magnification of 14,000 as described above. Using the point-counting method, we determined the nucleus volume to cell volume ratio and a nucleus surface to nucleus volume ratio as described (Weibel, 1979). Randomly chosen fields of cells containing ER or Golgi membranes were magnified to 31,000 to establish the ER(Golgi) volume to cell cytoplasm volume ratio by the point-counting method (Weibel, 1979). Some of these images were photoenlarged to 120,000 to determine the ER(Golgi) surface to volume ratio. The ER(Golgi) surface was found by formula 3. Corrections of bias due to section thickness were done as described (Weibel and Paumgartner, 1978). For the ER volume, the correction factor was 0.51 and 0.65 for the ER surface. Assuming that two-thirds

of the Golgi complex was composed of cisternae and one-third of tubules, the correction factors for Golgi volume and surface were estimated to be 0.6 and 0.64, respectively.

Estimation of Number and Density of Total ER-derived Buds. To estimate the number ER-derived buds, we used two distinct criteria: (*a*) a bud was considered an elevation on the surface of the ER with a width of 60–80 nm and covered with a characteristic coat on the external leaflet of the membrane; and (*b*) buds had a direct connection with the ER membrane and were extruded from the membrane by at least 50% of their circumference. The total number of ER buds per cell was determined as described (Lucocq et al., 1989). To obtain this value, we multiplied the total number of ER buds detected in thin-sections of ~300 cells by the mean volume of cells and divided that value by the total volume contributed by the ~300 cells. The latter value was found by multiplying the thickness of a section by the total surface area of the ~300 cell sections in which ER buds were counted.

By using relatively thick sections corresponding to the average diameter of an ER bud and the above two criteria, we were able to avoid double counting most of the ER buds present on consecutive thin sections. To establish this point independently, we performed a separate experiment in which the total number of ER buds was counted on several stacks of serial thin-sections. By comparing the number of ER buds determined by this reconstruction approach to the number determined by counting of individual sections (indirect method), we found that overestimation by the latter technique was <10–15%. Hence, both methods could be used interchangeably. We also found that the indirect method showed a high reproducibility. In spite of the high degree of ER bud enrichment in local zones, the comparison of estimates of the total number of buds per cells between groups of as few as 35 randomly taken cells with a total surface of section of 2,500 μm^2 gave a value of variance of less than 5% from one group to another. In addition, in four different experiments, the value of the total number of buds per cell was found to be the same. Because of technical simplicity, we routinely used the indirect method to estimate the average number of buds per cell.

Estimation of Number and Density of ER Membranes and ER-derived Buds in the Golgi Exclusion Zone. The Golgi exclusion zone is defined as the Golgi-containing region found in the pericentrosomal region of RBL cells and includes directly adjacent bud-bearing cisternae of the ER. The surface area of the Golgi exclusion zone in each individual section within a stack of 11–20 consecutive sections (referred to as a disector [Sterio, 1984; Lucocq et al., 1989]) was determined by the point-counting method (Weibel, 1979), and the mean surface area in each disector was calculated for 12 different cells (range from 30–90 μm^2). To find the volume of the Golgi exclusion zone included in the disector, the mean surface area of the Golgi exclusion zone in each disector was multiplied by the thickness of the section and the number of individual sections (35 to 105 μm^3 for 12 individual disectors). The total number of ER buds within each disector of a given cell was found by reconstruction from serial sections. The volumetric density of ER buds was calculated by dividing the number of buds found within each disector by the volume of the disector. The total volume and surface of ER membranes in the Golgi exclusion zone was found by the point-counting method (Weibel, 1979). By dividing the total number of ER buds by the ER surface within the Golgi exclusion zone, we calculated the density of ER buds in this region.

Estimation of Number and Density of ER Membranes and ER-derived Buds outside of the Golgi Exclusion Zone. The density of ER buds outside of the Golgi exclusion zone was found according to the procedure described above for the Golgi exclusion zone.

Estimation of Number and Density of ER Membranes and ER-derived Buds in Export Complexes. The local density of buds on individual cisternae associated with export complexes was determined as follows: using a stack of sequential serial sections, we followed one continuous bud-bearing zone of ER membrane that contained at least four buds. The distances between the most distant ER buds in the stack were directly measured in both the plane of the section and the depth of the stack. These two distances were multiplied by one another to get a surface area of the plane of the ER bud-bearing region. The total number of ER buds in such a zone (obtained by reconstruction as described above for the Golgi exclusion zone) was then divided by the area of the bud-bearing zone to determine a local ER bud surface density.

Estimation of Number of VTCs. The number of VTCs per cell was determined using the disector method (Sterio, 1984) as described (Lucocq et al., 1989). Sections of 26 random cells were photographed at a calibrated magnification of 7,000 throughout 25–35 consecutive sections in which they were present. Each "end section" was designated the "look-up" section, and all clusters present in the other sections, but not in the look-up section, were counted (Q). Then the volume of disector (V_{dis}) was determined by multiplying the average surface of individual cells in the stack found by the point-counting method by the depth of the dissector, which is equal to the thickness of the section multiplied by the number of sections in the disector. The total number of clusters in individual cells ($N_{clusters/cell}$) was determined by the formula,

$$N_{clusters/cell} = Vc.r. \times \Sigma Q / V_{dis}. \quad (4)$$

Total Number of Vesicular Profiles in VTCs. To determine the number of elements in VTCs, the value reported assumes that all elements found in consecutive sections are discontinuous with one another. This value is likely to be an overestimate, as some of the tubular structures within VTCs may extend across several sections. The number of elements in VTCs was determined by direct counting of individual profiles on each serial section. These were summed throughout all sections through a given VTC to obtain a total value.

Probability Measurements. To estimate the probability of a bud having proximity to a second bud in the cell, images of serial sections were photoenlarged to 40,000 to reconstruct a section of the cell in three dimensions. 300 randomly chosen ER buds were taken as the center of reference (referred to as reference buds), and the distance between each individual reference bud and other ER buds in the same and consecutive serial sections encompassing up to 1.3 μm distance above and below the reference bud was measured directly. A series of concentric shells with a volume equal to the volume of the most internal sphere having a 0.2-μm diam (corresponding to a volume of 0.0042 μm^3) was constructed around the reference bud. Subsequently, each measured bud was assigned to a shell with its distance from the reference bud being that of the corresponding outer diameter of the shell. The probability of finding a bud within a particular shell was determined by dividing the number of positive shells by the number of reference buds, and the value was reported as a percentage.

SEM. Statistical calculations were performed by determining the SEM for the pooled stereological data for each condition as described in the Results.

Immunolabeling of Cryosections

NRK cells grown on 35-mm tissue-culture dishes were infected with vesicular stomatitis virus (strain ts045), postinfected for 4 h at 39.5°C, and permeabilized as described (Plutner et al., 1992). After incubation at the permissive temperature (32°C) as described in the Results, the cells were fixed for 30 min with 3% paraformaldehyde and 0.1% GA in PBS (pH 7.4), washed for 10 min in PBS containing 0.05 M glycine, scraped, mixed with a preheated (40°C) 10% gelatin in PBS, and centrifuged at 15,000 *g* in a microcentrifuge for 10 min. Cells embedded in gelatin were cooled on ice, and a solid pellet was cut into 1-mm-wide cubes. After overnight cryoprotection by infiltration with a mixture of 2.3 M sucrose in 0.1 M phosphate buffer (pH 7.4) containing 20% polyvinyl pyrrolidene, the cubes were mounted on aluminum nails and frozen in liquid nitrogen. Ultrathin cryosections cut on a Reichert Ultracut E, equipped with a FC-4 cryoattachment, were picked up with 2.0 M sucrose–1% BSA in PBS and collected on Formvar/carbon-coated nickel grids. Sections were then quenched in 0.01 M glycine in PBS, incubated for 30 min in 10% FBS-PBS at rt, and for 1–2 h with primary antibodies diluted in 10% FBS-PBS antibody. Excess primary antibody was removed by multiple rinses in 5% FBS-PBS, followed by transfer of the section to a drop of 10% FBS-PBS containing 6 or 10 nm gold–conjugated anti–rabbit antibodies. After a 2-h incubation at rt, the grids were washed in double-distilled water and stained in 2% neutral uranyl acetate (10 min), followed by embedment in 3.2% polyvinyl alcohol/0.2% methyl cellulose, containing 0.2% uranyl acetate. No labeling was observed in controls in which primary antibodies were omitted.

Immunolabeling of VSV-G Using the Immunodiffusion Approach and Quantitation of VSV-G Concentration in VTCs

NRK cells were infected with ts045 VSV as described above. After digitonin permeabilization (Plutner et al., 1992) and incubation in vitro as described in the Results, cells were fixed with 0.025% GA/3% paraformaldehyde for 30 min. Cells were washed three times with PBS, quenched with 0.05 M glycine in 10% FBS/PBS for 30 min, and incubated overnight with an anti–VSV-G cytoplasmic tail mAb (P5D4) (Kreis, 1986). Cells were washed twice with FBS/PBS, followed by incubation with rabbit anti–mouse antibodies for 1–2 h and with 6 or 10 nm gold conjugated to anti–rabbit antibodies for 2 h. Excess unbound antibodies were removed by washing, and the cells were fixed with 2.5% GA for 30 min. Cells were

scraped, pelleted, and processed for Epon embedding. For three-dimensional visualization using quick-freeze, deep etch replicas, immunolabeling was performed on glass coverslips.

For quantitation, the Epon-embedded cell pellet was cut as described above. Images (×10,000) were scanned into a computer, and membrane outlines of the ER and VTCs were measured using the program NIH Image, version 5.9. The linear density of gold particles corresponding to VSV-G was determined as described (Balch et al., 1994). For determination of the distribution of vesicles and VTCs, NRK cells grown on glass coverslips were permeabilized and incubated as described in the Results, fixed and labeled for VSV-G using the immunodiffusion protocol, and embedded in Epon on the glass coverslip as described above. After detachment from glass, thin layers of cells embedded in Epon were sandwiched against each other and reembedded in Epon. Vertical sections of cells were prepared and counterstained as described above. ER to Golgi intermediates were identified based on either the presence of gold particles corresponding to VSV-G or on their characteristic morphology as described in the Results.

Preparation of Quick-Freeze, Deep-Etch Rotary-shadowed Replicas

After incubation in vitro as indicated in the Results, semi-intact cells grown on 9 × 9 mm glass coverslips were fixed in 2.5% GA in PBS for 1 h, washed in PBS, and divided into small pieces (~3 mm^2). Coverslips were rinsed exhaustively in double-distilled water, followed by a rinse with 10% methanol in water, and quick-frozen using a liquid nitrogen–cooled copper block gravity press (Hitek, Benicia, CA). The cells were fractured with a razor blade under liquid nitrogen, freeze dried in a vacuum evaporator (400; Balzers, Inc., Lichtenstein) and replicated with ~2 nm of platinum that was rotary deposited from 24° above the horizontal. The replica was then reinforced with ~140 Å of carbon using an electron gun at an angle of 90° to the horizontal. A drop of 2% colloidion solution was applied on the replica membrane. The coverslips were detached in a 40% solution of hydrofluoric acid, and cells were dissolved in Chlorox. After washing, replicas were transferred to Formvar-coated copper grids, the colloidion film on replicas was dissolved with amylacetate, and images were examined using TEM.

Results

ER-budding Activity Is Enriched within the Vicinity of the Golgi Apparatus

The basic stereological parameters of the RBL and NRK cell line used in these studies are shown in Table I. To morphometrically evaluate the distribution of export sites, ER-budding structures were identified as an elevation on the surface of the ER with a width of 65–85 nm, extruded from the membrane by at least 50% of their diameter, and covered with a distinctive electron-dense coat (Fig. 1–3, *arrowheads*). Budding sites emanate from three locations in the cell including (*a*) those associated with the nuclear envelope (Fig. 1), (*b*) those associated with the Golgi apparatus that are analogous in structure to classical ER transitional elements (Palade, 1975; Sesso et al., 1994) (Fig. 2), and (*c*) those found in more peripheral regions that lack detectable Golgi (Fig. 3).

*Table I. Basic Morphometric Parameters of NRK and RBL Cells**

	Cells	Nucleus	ER	Golgi
NRK				
Volume (μm^3)	1,205 ± 43	260 ± 14	37.8 ± 2.3	7.8 ± 0.7
Surface (μm^2)	3,868 ± 127	262 ± 13	2,448 ± 138	512 ± 42
	$n^{\ddagger}$ = 569	n = 185	n = 48	n = 105
RBL				
Volume (μm^3)	780 ± 38	217 ± 12	20.3 ± 1.5	4.3 ± 0.4
Surface (μm^2)	665 ± 27	176 ± 9.6	2,031 ± 90	183 ± 16
	n = 113	n = 113	n = 56	n = 113

*All data were determined as described in Materials and Methods.
‡n, number of cells counted.

Buds found at the tip of tubular projections from the surface of the ER had an average diameter of 78 ± 6 nm. Although tubular projections were generally shorter than 150 nm (Fig. 1, section 5; *arrowheads*), they could be as long as 350 nm based on reconstruction from serial-thin sections. Buds were covered with an ~8–10-nm-thick electron-dense coat. On grazing sections and at high magnification, the coat of ER buds possessed a lattice-like appearance due to a semi-regular array of 4–5-nm elongated particles (Fig. 1, *inset*). These coats are similar to those observed in pancreatic acinar cells (Merisko et al., 1986). Based on analysis of random sections through ~300 cells (see Materials and Methods), the average number of buds in a cell was found to be 250 ± 10. 45% of budding profiles were found on ER tubules located in the vicinity of Golgi complexes, whereas 55% were located in regions without noticeable juxtaposition to Golgi. 11% of total buds were observed emerging from the nuclear envelope. Thus, it is apparent that a substantial level of membrane exiting the ER appears to do so from sites distant from Golgi elements.

The overall average density of total ER buds based on the cross-sectional volume of the cytoplasm was found to be 0.5 buds per μm^3, or 0.14 buds per μm^2 of total ER surface. However, the average density of ER-budding profiles found within the pericentrosomal area containing the Golgi apparatus (referred to as the Golgi exclusion zone) was five- to sevenfold higher (3.3 buds per μm^3 of cytoplasm or 0.8 buds per μm^2 of ER surface) than the average value found on the total ER membrane. Outside of the Golgi region, the overall mean density was 1.5–3-fold lower (0.22 buds per μm^3 cytoplasm or 0.04 buds per μm^2 of ER surface) than the average values found for the cell. The markedly increased budding density around the Golgi apparatus is consistent with the highly focused export activity observed from ER transitional elements present in the Golgi region of pancreatic acinar cells (Palade, 1975).

Figure 1. Export sites adjacent to the nuclear envelope of RBL cells. Six consecutive serial sections through a VTC adjacent to the nuclear envelope. ER buds (*arrowheads*) emerging from the nuclear envelope (section *1*) and parallel ER membrane (*stars* in section *2–6*) are facing VTCs. (*Inset*) Higher magnification view of two ER buds. The slice of the section presented in the inset encompasses either only the coat (*right*), or both the coat and the membrane and the luminal part of a bud (*left*). Individual 4–5-nm electron-dense particles arranged in a semiregular pattern (*arrows*.) Notice the same appearance of the coat under lower magnification of serial sections that contain a honeycombed appearance consisting of a semiregular array of electron-dense particles (*arrows*). Adjacent to buds, we observe a typical pleomorphic element (*large asterisk* in section *5*) within a VTC that has numerous tubular projections (*small asterisk*) in adjacent thin-sections (*small asterisks* in sections *4* and *6*), indicative of its fenestrated structure. Tubules in the fenestrated elements of the VTC possess a dark dense coat (*arrows* in sections *4* and *6*) typical of those found on Golgi compartments and are readily distinguishable from the alveolate coat associated with COPII buds emanating from the ER. Bar, 0.1 μm.

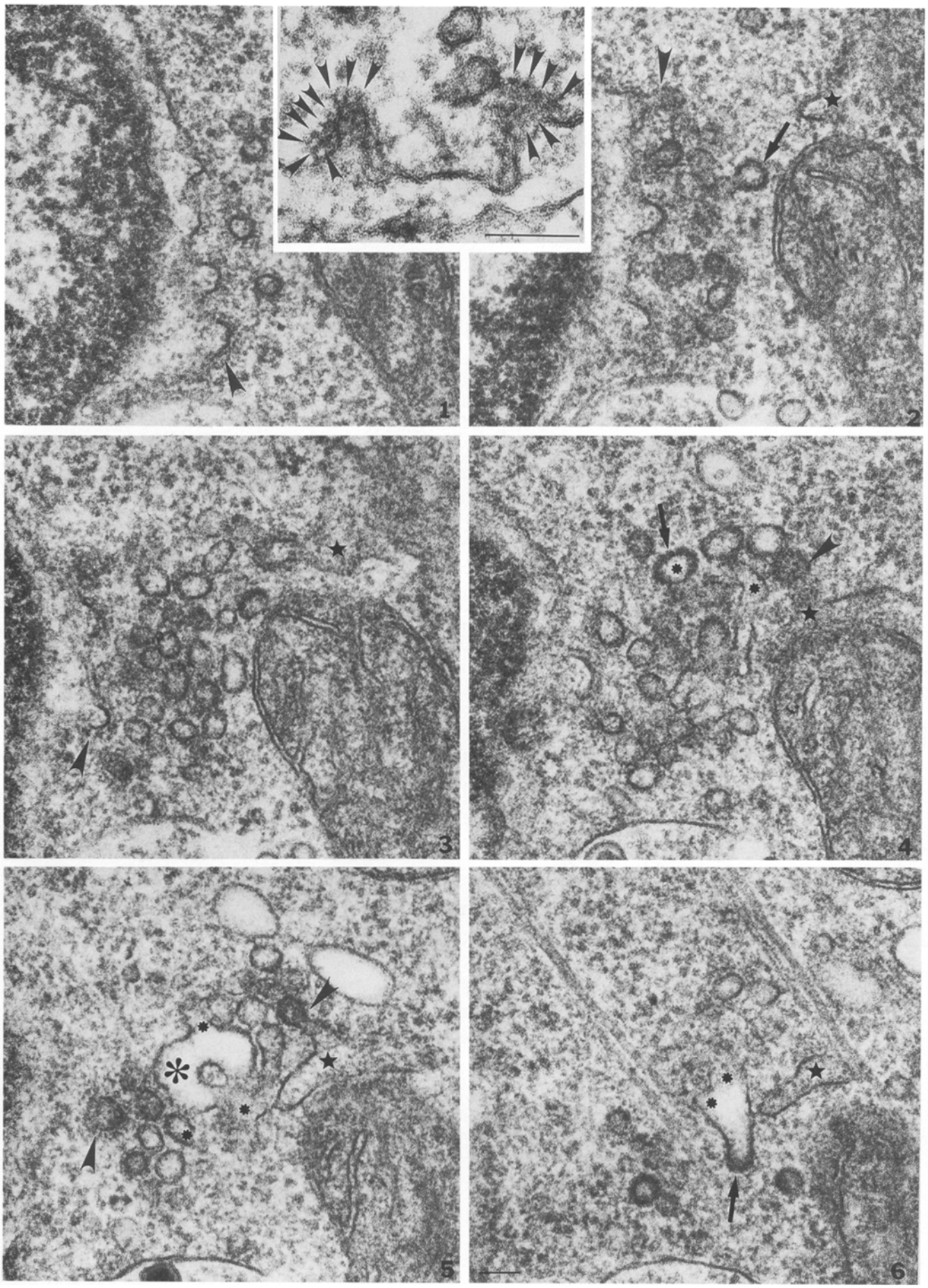

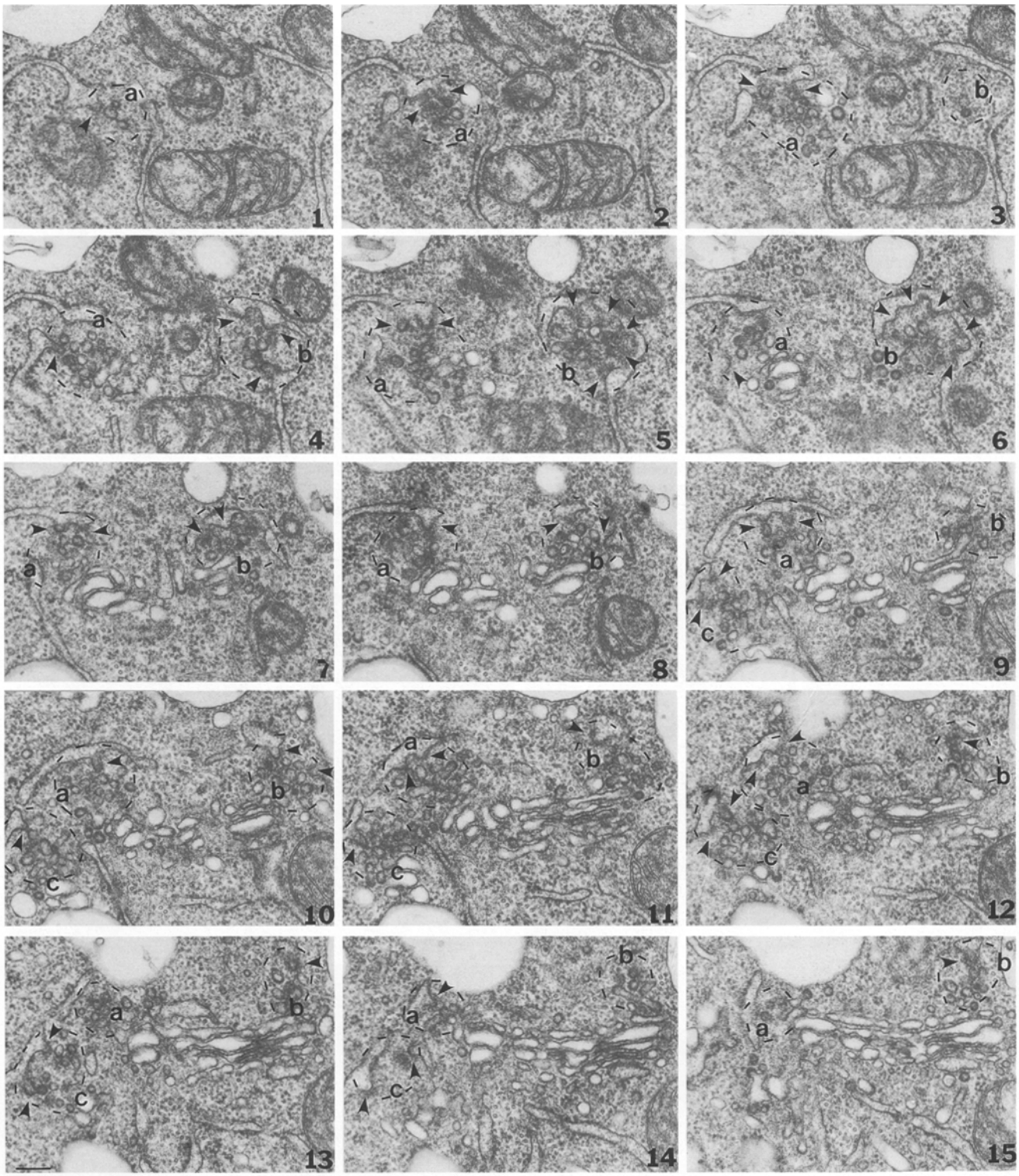

Figure 2. Export complexes adjacent to the pericentrosomal Golgi region of RBL cells. 15 consecutive serial sections through three (*a*, *b*, and *c*) Golgi-adjacent export complexes (*encircled by dotted lines*) are shown with ER buds (*arrowheads*). Export complex *a* contains 13 ER-derived buds, export complex *b* contains 11 buds, and export complex *c* contains seven buds. Note the characteristic cup-shaped appearance of ER bud-bearing zones especially evident for export complex *b*.

ER-budding Activity Is Also Enriched in Peripheral Export Complexes

To develop a detailed understanding of the topological organization of ER export throughout the cytoplasm, we carried out a morphological reconstruction of those sites that were not adjacent to Golgi elements, referred to as peripheral sites. An analysis of peripheral sites allows us to discriminate the structure of ER-derived intermediates

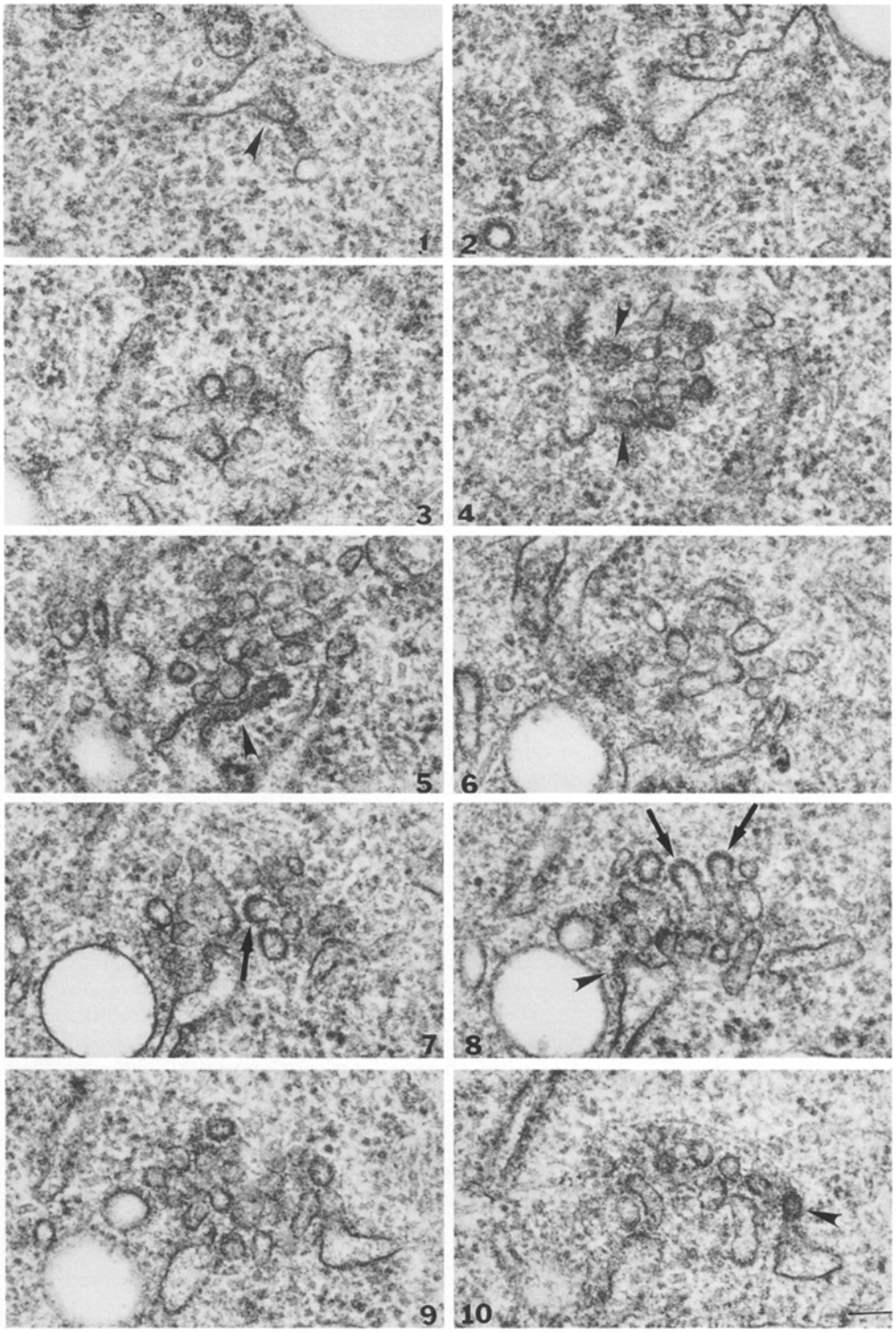

Figure 3. Export sites in peripheral regions of the cell cytoplasm that are distant from Golgi stacks. 10 consecutive serial sections through a peripheral export site of RBL cells are shown with ER buds (*arrowheads*). ER strands bearing nine buds partially surround the VTC. Tubular elements of the VTC possess a Golgi-like uniform, dense, thick coat (*arrows* in sections *7* and *8*). Bar, 0.1 μm.

from that of the fenestrated *cis*-Golgi network (CGN), which is always associated with ER buds near the Golgi. ER buds on peripheral sites (Fig. 3) typically emanated from short stretches of ER membrane. These regions were separated by long distances from other similar budding foci. Frequently, ER buds found on different cisternae were closely juxtaposed and faced each other. These features are more evident in Fig. 4 (*A* and *B*), which presents an overlapping reconstruction of serial sections of the peripheral site shown in Fig. 3. Budding profiles (*blue*) protrude from the ER (*green*) into a central region containing a collection of vesicles and tubular elements comprising VTCs (*red*). This typical organization of peripheral sites is also characteristic of budding sites associated with the nuclear envelope (Fig. 1) and budding sites adjacent to the Golgi stack (Fig. 2). The close topological relationship between ER buds and distinct VTCs suggests that these structures function as a compact morphological unit that we now refer to in its entirety as an export complex.

Morphometric analysis of peripheral export complexes

revealed that these sites typically contained two to six buds emanating from the ER, although this could approach a value of 20 for some exceptional, larger clusters (Fig. 5 *A*, *closed circles*). These sites had an average number of buds per site of 4.4 ± 0.3 (Table II), a value that was slightly smaller than the average number of buds per site found in export complexes adjacent to Golgi (6.1 ± 0.4 buds per site; Table II). By including only ER-budding profiles facing VTCs, we were able to estimate a "local" bud density in these export complexes. On average, this value was 17.2 ± 2.5 buds per μm^2 of ER surface, which, on a relative scale, is 125 times higher than the average bud density found on the total ER surface (0.14 buds per μm^2) and approximately five times higher than the bud density found on the surface of the ER within the Golgi exclusion zone.

Buds Are Formed Nonrandomly along the ER Surface

The apparent nonrandom distribution of ER buds led us to quantitatively estimate the probability of a given bud having proximity to a second bud in the cell. For this purpose, we constructed a series of concentric shells of equal volume that radiate outward from the center of randomly chosen buds. The radius of the first internal shell was arbitrarily assigned a value of 0.1 μm to encompass the entire tip of a budding structure. Each increment in the diameter of successive shells extending outward from the first shell progressively decreased in dimension to encompass the same volume in three-dimensional space. Given the average number of buds in a cell (~250), the volume of cell cytoplasm (560 μm^3), and the volume of a shell (4.2×10^{-3} μm^3), if buds assumed a strictly random distribution, then the probability of encountering another bud in a given concentric shell would remain equal with a value of 0.18% (Fig. 6, *diamonds*). However, if buds were confined to regional foci, the probability of encountering a second bud would be high in the first series of concentric shells, and then fall off very rapidly with increasing distance in three-dimensional space.

The results of such an analysis are shown in Fig. 6 where we have plotted the probability of encountering a bud relative to its location in sequential concentric shells of equal volume (Fig. 6, *open circles*), or relative to the diameter of the outermost surface of a given shell in which a bud is found (Fig. 6, *closed circles*). It is clear that the distribution did not follow that predicted for a strictly random budding event. The probability of detecting a second bud within the first 50 consecutive shells having up to a 0.6-μm outer shell diameter markedly exceeded that of a random distribution (Fig. 6). After a plateau at a value similar to that calculated for a random distribution (up to an outer diameter of 0.8 μm or 100 shells), the probability fell dramatically within the three-dimensional space defined by the outermost shell examined (~1.2 μm). We conclude that budding is not a random event along the surface of the ER, but rather is remarkably restricted to regional hot spots of budding activity associated with export complexes.

Structural Organization of Export Complexes In Vivo

As illustrated in Fig. 4, ER-budding profiles predominately faced into an area filled with VTCs in vivo. VTCs, defined as a group of four or more 60–80-nm vesicular profiles with a characteristic shape and coat, were never detected in regions lacking adjacent ER buds. The membrane profiles of VTCs were distinct from the ER and found to be more variable in size compared to the rather homogeneous appearance of buds emanating from the ER surface. The average diameter of VTCs based on serial-thin sections was found to be ~0.4 μm (Table II) with a range that varied from ~0.2 μm to >1 μm (Fig. 5 *B*). Although technical limitations do not allow us to make a complete three-dimensional reconstruction of membrane continuities between elements of VTCs, individual profiles often appeared to be continuous in several consecutive sections and consisted of short tubules that could be connected together in a more fenestrated structure (Fig. 1, *asterisks*). Tubules within VTCs characteristically had a dense COPI-like coat at their tips (Figs. 1 and 3, *arrows*) (Melancon et al., 1987; Orci et al., 1993*a*). The presence of a COPI-like coat within VTCs is consistent with the numerous morphological studies that have demonstrated that these pre-Golgi intermediates are a major site of COPI localization when examined using indirect immunofluorescence (Lippincott-Schwartz, 1993; Aridor et al., 1995) or TEM (Oprins et al., 1993; Pind et al., 1994*a*; Griffiths et al., 1995*b*).

To estimate the total number of elements within a VTC, we assumed that each profile appearing in an individual section was, in fact, a separate vesicle or tubule. From this assumption, the average number of elements was determined to be 32 ± 4 (Table II). Clusters generally contained between 10 and 60 vesicular-tubular elements, although some of the clusters contained as many as 150 elements (Fig. 5 *C*). Although these values are undoubtedly an overestimate of the total number of luminally distinct elements, given that tubules within VTCs are likely to extend across several consecutive thin-sections, they serve as a useful numerical approximation for the relative size and composition of VTCs. When we compared the number of elements found in peripheral vs Golgi-adjacent VTCs, we observed very similar values, suggesting they are of comparable size (Fig. 5 *C*). Whereas peripheral VTCs were generally spherical in shape, those adjacent to Golgi possessed a semispherical shape with the CGN occupying one hemisphere, and the other hemispheres facing ER membranes. Using the disector method to estimate the total number of VTCs per cell (Sterio, 1984) (see Materials and Methods), we found an average value of 74 ± 11 clusters per cell. This level is similar to that observed using more indirect TEM methods (Buccione et al., 1996) or indirect immunofluorescence in other cell lines (Plutner et al., 1992; Aridor et al., 1995).

Biochemical Requirements for the Generation of Export Complexes In Vitro

To correlate our morphological observations with previous in vitro biochemical studies, we used semi-intact NRK cells to examine the potential role of COPII components in the formation of ER-derived buds and VTCs (Plutner et al., 1992; Peter et al., 1993; Balch et al., 1994; Pind et al., 1994*b*). Semi-intact cells incubated for 30 min at 32°C in

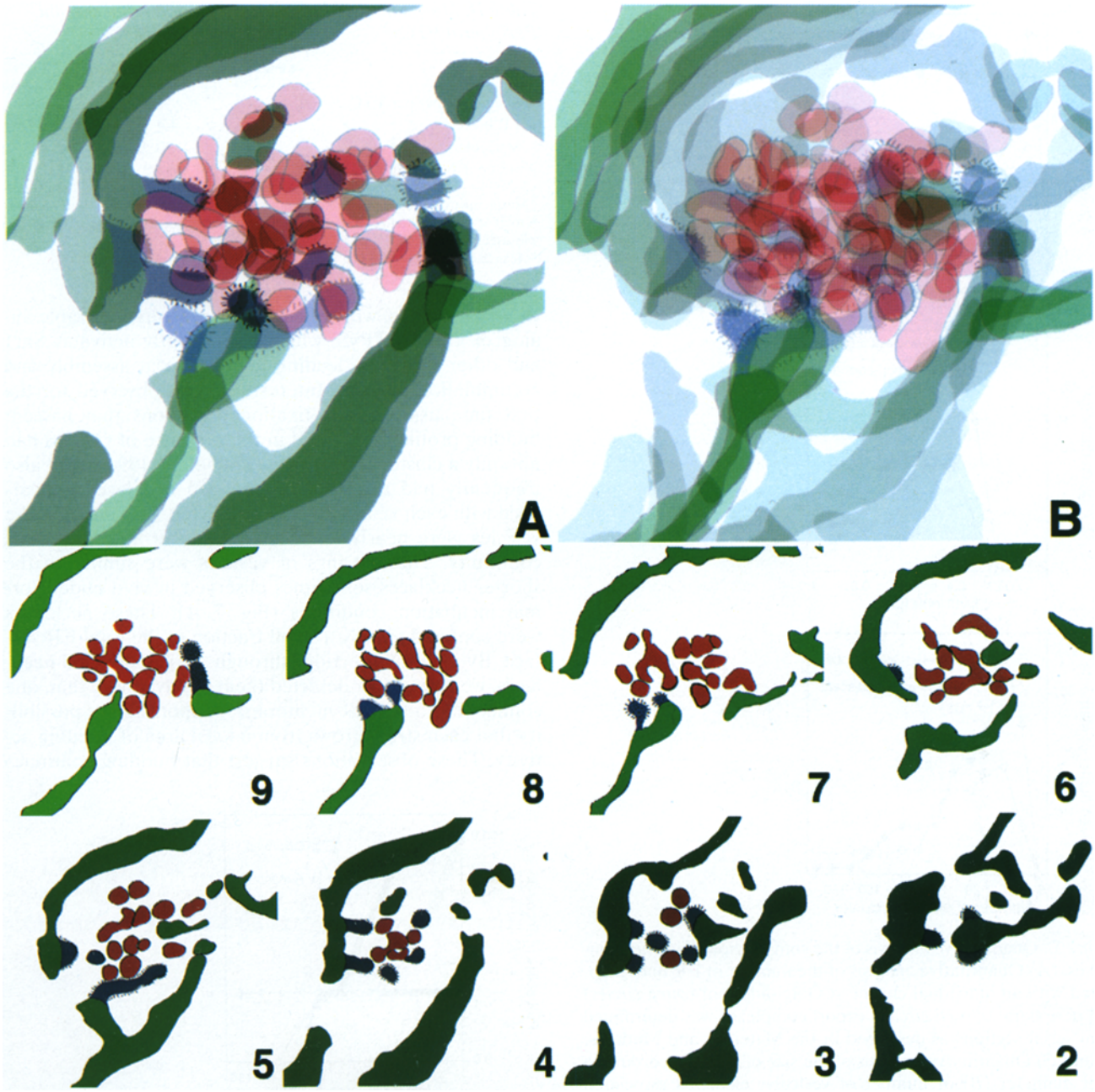

Figure 4. Three-dimensional reconstruction of a peripheral export complex. Membrane contours shown in Fig. 3 are illustrated at a magnification of 160,000. Transparencies containing the membrane contours were scanned, overlayed, and coaligned based on the position of mitochrondria and ER. Green denotes ER cisternae, blue denotes ER buds, and red denotes tubules and vesicles of VTCs. Vesicular membrane contours within the VTC whose luminal continuity to the surrounding ER membranes was evident in consecutive sections were denoted in green. More intense shades of the same color reflect distance from the uppermost section. The alveolate coats of ER buds, where evident, are dictated by stipples. Images are presented either individually with the section number indicated (*bottom two rows*), or as an overlay containing four images (*left*) for clarity or all eight images (*right*). The resulting reconstruction shows the clustered structure of a typical VTC, surrounded by ER-bearing buds occasionally penetrating the periphery of a VTC, as evidenced by the coated portions of ER tubules (*blue*) adjacent to VTC tubules (*red*).

the absence of cytosol failed to generate detectable VTCs (not shown). This result is consistent with the fact that preexisting VTCs are unstable during permeabilization (Aridor et al., 1995) and that cytosol contains essential soluble components of the COPII machinery required for the export of cargo from the ER (Barlowe et al., 1994; Kuge et al., 1994). VTCs generated in vitro in the presence of cytosol are nearly identical to those observed in vivo. We have previously shown that they are composed of a compact network of tubules and vesicles that lack direct luminal connections to ER membranes and frequently label positively for β-COP using immunoelectron microscopy (Balch et al., 1994; Pind et al., 1994*a*). However, ER-budding profiles, like those observed adjacent to VTCs in vivo (Figs. 1–3, *arrowheads*), were rarely observed in vitro. Since previous studies used mild fixation conditions in conjunction

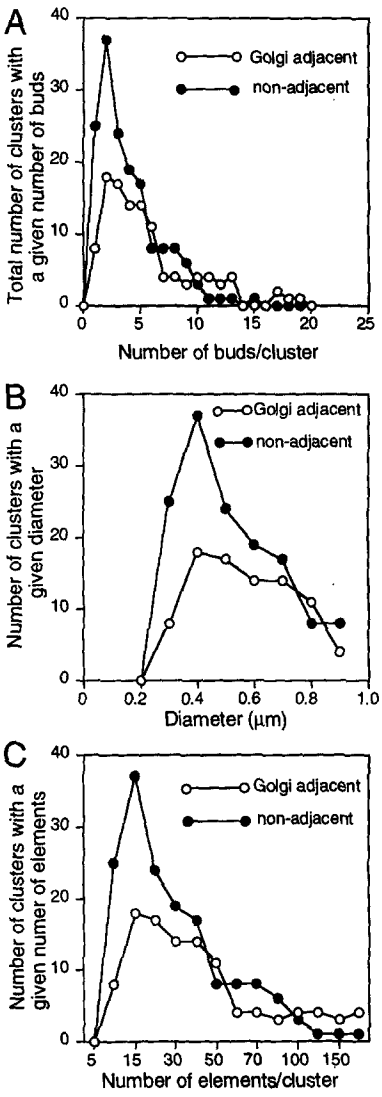

Figure 5. Quantitative analysis of the composition of export complexes. (*A*) Quantitative analysis of the number of ER buds associated with an individual cluster in Golgi-adjacent (*open circles*) and peripheral (*closed circles*) export complexes was determined from serial sections as described in the Materials and Methods. (*B* and *C*) Quantitative analysis of the size of VTCs according to their diameter (*B*) or number of vesicular elements associated with a VTC (*C*) was determined by reconstruction of serial sections from Golgi-adjacent (*open circles*) and peripheral (*closed circles*) structures as described in the Materials and Methods. Data were collected from complete reconstructions of 116 Golgi-adjacent and 164 Golgi-peripheral export complexes in RBL cells.

with an immunodiffusion procedure to label VSV-G in VTCs (Balch et al., 1994), we reasoned that ER buds may be labile structures. We therefore applied more stringent fixation and embedding conditions to preserve ultrastructural details (see Materials and Methods). Under these conditions, ER buds were observed that had a characteristic coat resembling those found in vivo and were only detected adjacent to VTCs (not shown), suggesting that even in semi-intact cells, budding is restricted to specialized regions of the ER.

To examine the formation of buds and their relationship

*Table II. Morphometric Parameters of Golgi-adjacent and Peripheral VTCs**

	Golgi-adjacent	Peripheral	Total
Average number per VTC:			
ER buds	6.0 ± 0.4‡	4.4 ± 0.3	5.1 ± 0.3
Vesicular elements	35 ± 3	30 ± 3	32 ± 3
Average diameter of VTC (μm)	0.40 ± 0.06	0.39 ± 0.06	0.39 ± 0.06

*Morphometric parameters were determined as described in Materials and Methods. A total of 116 Golgi-adjacent and 163 peripheral reconstructions of export complexes was used in generating the data shown.
‡Mean ± SEM.

to VTCs in vitro, we made use of the nonhydrolyzable analog of GTP, GTPγS, which permanently activates Sar1 and other GTPases, leading to stable coat assembly and accumulation of buds. Interestingly, we observed for the first time using strong fixation conditions that nascent budding profiles generated in the presence of GTPγS had not only a cluster appearance (Pind et al., 1994*a*), but also frequently had a distinctive "beaded necklace" appearance with each vesicle being a bead (Fig. 7, *B* and *C*). The vesicles were nearly identical in size but lacked luminal continuity. These strings of vesicles were similar to the shorter necklaces sometimes observed in vivo under normal incubation conditions (Fig. 7 *A*). These necklaces were confined to only a small fraction of the total ER surface. By analyzing sections through >600 individual necklaces, we have never detected them to have more than one connection to the ER membrane, supporting the possibility that each string grows from a local area of budding activity. These observations suggest that budding continues

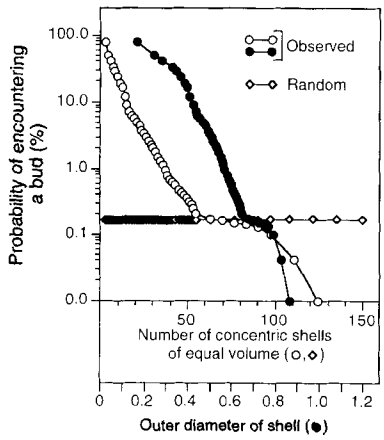

Figure 6. Probability of a given bud having proximity to a second bud in the cell. Randomly chosen ER buds present in RBL cells were assigned as the center of reference, and distances between it and any other buds present in 30 consecutive serial sections were determined by building a series of concentric shells with a constant volume of 0.0042 μm^3, corresponding to the volume of the first internal shell having a diameter 0.2 μm (to encompass a single bud) as described in the Materials and Methods. The probability was determined by counting the number of buds detected in each shell relative to the total number of buds detected (percentage of total). This value is plotted as shell number in which a second bud was found (*open circles*) or relative to the outermost diameter of a particular shell (*closed circles*). The calculated probability of a second bud having a completely random distribution in the cell (0.18%) is presented for comparison (*diamonds*).

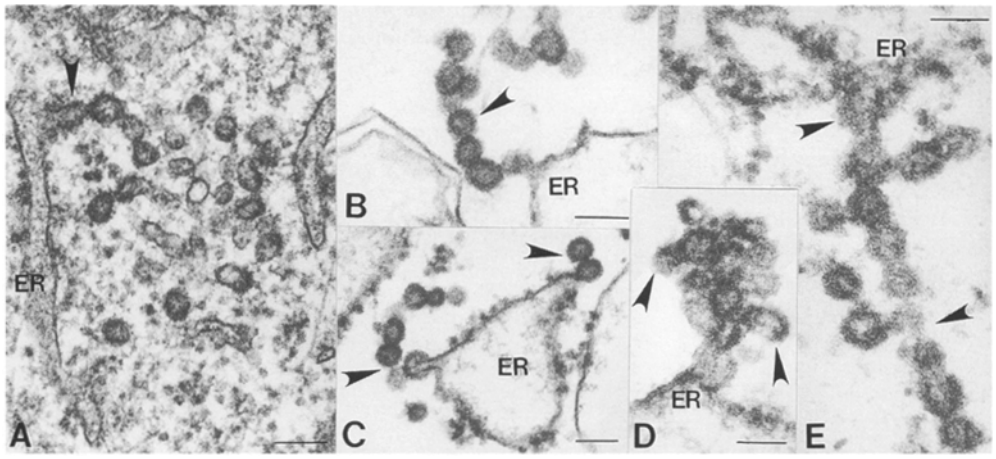

Figure 7. Morphological features of ER-derived buds observed in vivo and in vitro. (*A*) Buds protruding from the ER of RBL cells in vivo (*arrowhead*) show a necklace-like appearance with two to three incompletely pinched-off vesicles remaining attached to the single bud protruding from the ER. (*B*) Semi-intact NRK cells were incubated in vitro in the presence of cytosol and ATP as described in the Materials and Methods. Note that buds (*arrowheads*) can be readily detected protruding from ER-like elements. (*C*) ER buds and vesicles (*arrowheads*) formed in vitro in the presence of GTPγS show a zig-zag appearance with occasional singular branches (*arrows*). (*D* and *E*) ER buds accumulated in the presence of the GTP-restricted Sar1[H79G] mutant can form grape-like groups (*D*) or a highly branched network (*E*). (*Arrows*) Single branches. Bar, 0.05 μm.

in the absence of GTP hydrolysis, but that the vesicles fail to complete separation from one another. Upon immunolabeling, we found accumulated vesicles to be substantially enriched in VSV-G (Pind et al., 1994*a*) and components of both COPI (β-COP) (Pind et al., 1994*a*; Griffiths et al., 1995*b*) and COPII coats (Sec13 and Sec 23) (Fig. 8, *A–C*).

To establish that necklaces formed in response to a specific block in COPII coat disassembly, we examined the effect of an activated, GTP-restricted mutant of Sar1, Sar1[H79G], which promotes vesicle accumulation in vivo and in vitro (Aridor et al., 1995; Kuge et al., 1994). Examination using strong fixation conditions revealed a striking similarity to GTPγS-formed structures. Vesicles were detected as both clusters (Fig. 7 *D*) or as necklaces (Fig. 8 *E*) emerging from restricted regions of the ER. As expected, coats were enriched in the COPII components Sec13p

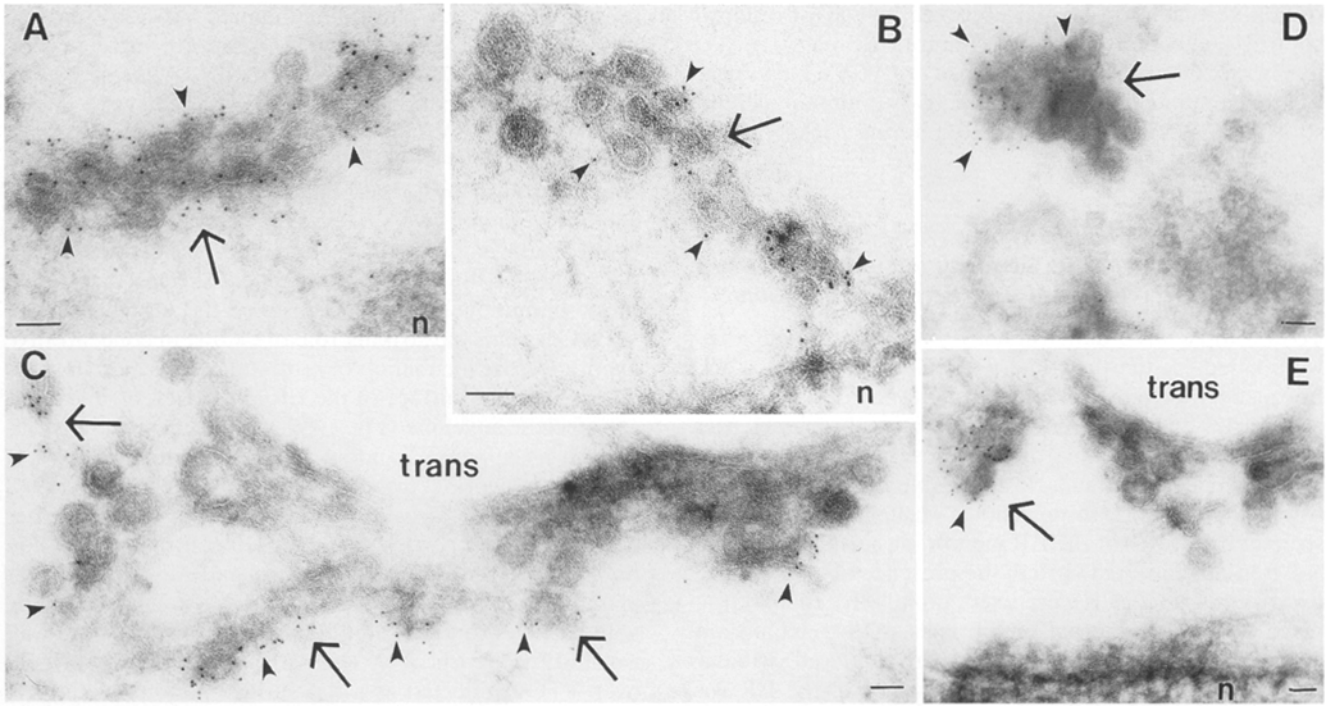

Figure 8. ER buds formed in vitro in the presence GTPγS or the Sar1-GTP–restricted mutant contain components of COPII coats. Semi-intact NRK cells were incubated in vitro, and cryosectioning and immunolabeling of cell pellets were as described in Materials and Methods. Clusters of vesicles (*arrows*) accumulated in the presence of GTPγS (*A*, *B*, and *C*) or Sar1[H79G] (*D* and *E*) contain Sec13p (*arrowheads* in *A*, *C*, and *D*) and Sec23p (*arrowheads* in *B*, and *E*) as shown by the distribution of gold particles using specific antibodies. Note that the cisternal portion of the Golgi apparatus with the *trans* face labeled in *C* and *F* remains unlabeled by Sec13p- and Sec23p-specific antibodies, whereas clusters (*arrows*) that are closely adjacent to the Golgi complex contain both Sec13p and Sec23p (*C* and *F*). Bar, 0.05 μm.

(Fig. 8 *E*) and Sec23p (Fig. 8 *F*). No COPI staining could be detected using an antibody specific for β-COP in these structures (not shown) (Aridor et al., 1995).

To examine the role of COPII in VSV-G concentration and the appearance of VTCs in export complexes, we used semi-intact cells infected with a temperature-sensitive form of VSV-G whose transport is blocked at the restrictive temperature (39.5°C) (Lafay, 1974; Plutner et al., 1992). Transfer of cells to the permissive temperature (32°C) results in the migration of a synchronous wave of ts045 VSV-G from the ER to VTCs and subsequent Golgi compartments (Plutner et al., 1992; Balch et al., 1994). After incubation at 32°C in vitro, cells were fixed and stained with an antibody specific for the cytoplasmic tail of VSV-G using the immunodiffusion protocol (Balch et al., 1994). As shown in Table III, incubation in the presence of wild-type Sar1 had little effect on ER export as judged by the abundance of VTCs detectable in vitro. In contrast, the guanosine diphosphate (GDP)–restricted form of Sar1 (Sar1 [T39N]) drastically reduced the formation of vesicles and VTCs (Table III), demonstrating the essential need to activate Sar1 to promote membrane flow from the ER through export complexes. In contrast, incubation in the presence of the GTP-restricted mutant (Sar1[H79G]) caused a dramatic accumulation of vesicles in clusters and an approximate twofold increase in the apparent number of clusters per section that could be detected (Table III).

When we determined the density of VSV-G in clusters formed in the presence of the Sar1-GTP restricted mutant, it was approximately five- to sixfold higher than that found in the ER before incubation (Table III). This fold-concentration was identical to that observed in VTCs present in control incubations lacking inhibitors (Table III). The five- to sixfold increase in the density of VSV-G in vesicles that accumulate in the presence of the mutant demonstrates that VSV-G is concentrated during packaging into COPII-coated vesicles.

Table III. Effect of Sar1 Mutants on the Concentration of VSV-G and the Organization of ER-derived Clusters during Export from the ER In Vitro

Protein	Average number vesicles per μm^3 of cytoplasm	Number of vesicles per cluster in each section[§]	Number of clusters per μm^3 of cytoplasm[‖]	VSV-G density (fold over ER)[¶]
Control (no additions)	2.8 ± 0.3*	9.3 ± 0.9	0.3 ± 0.1	5.9 ± 0.7
Sar1 wild type	1.7 ± 0.2	7.1 ± 0.7	0.2 ± 0.1	5.3 ± 0.5
Sar1[T39N]	0.2 ± 0.1	3.6 ± 0.4	0.05 ± 0.01	4.6 ± 1.3
Sar1[H79G]	6.6 ± 0.6	13.0 ± 1.3	0.5 ± 0.1	5.3 ± 0.3
GTPγS	5.2 ± 0.5	11.3 ± 1.2	0.5 ± 0.1	5.2 ± 0.3

*Mean ± SEM.
[‡]Density of ER-derived vesicles per μm^3 of cytoplasm was determined as described in the Materials and Methods.
[§]Total number of elements in clusters (determined as described in the Materials and Methods) was divided by total number of clusters detected.
[‖]Density of clusters determined as described in the Materials and Methods.
[¶]Fold-concentration of VSV-G over that observed in the ER was determined using immunoelectron microscopy as described in Materials and Methods.

Visualization of ER Export by a Three-dimensional Technique Confirms the Organization of Export Complexes Reconstructed from Serial Thin-Section

To develop a three-dimensional view of export complexes, we applied for the first time a modification of the quick-freeze, deep-etch methodologies used previously to visualize vesicles budding from the plasma membrane (Heuser, 1980) and Golgi compartments (Weidman et al., 1993). The approach is particularly applicable to semi-intact cells where the cytosol can be readily washed away to reveal structural features of the ER membrane surface.

After incubation in vitro in the presence of ATP and cytosol, semi-intact cells were fixed, rapidly frozen, and fractured to expose internal membranes. After etching and replication, intracellular organelles are rendered visible as three-dimensional structures. The surface of the ER was readily distinguishable from other subcellular compartments by the presence of ribosomes or, in the case of the nuclear envelope, additionally, nuclear pores. Adjacent to the surface of the ER, we frequently observed compact structures of similar size and apparent vesicular-tubular composition to VTCs observed in thin-sections (Fig. 9 *A*). These structures were completely absent in incubations that lacked cytosol or ATP. They varied in diameter, but were generally ~0.3–0.5 μm across and ranged from a circular to a more oblong shape under normal incubation conditions. Assuming that the distinctive ~80-nm surface undulations correspond to vesicle profiles (Fig. 9 *A*) and that a cluster can be represented as a sphere with a similar range of diameters, we estimate that VTCs detected in replicas could contain 50–110 individual elements. This value is compatible with the number of vesicular profiles determined by reconstruction from serial thin-sections.

To identify whether the above structures formed in the presence of cytosol and ATP contained ER-derived cargo proteins such as VSV-G, NRK cells were infected with ts045 VSV at the restrictive temperature. After permeabilization and incubation in vitro at 32°C, cells were immunolabeled for VSV-G using the immunodiffusion protocol (Balch et al., 1994) and replicas were prepared. While a combination of prolonged incubation using mild fixation conditions to label VSV-G and the presence of prominent "gold shadows" from the etching and replication reduces the ability of the technique to reveal surface features of these immunogold-labeled clusters, the distribution of VSV-G reveals the striking role of COPII in concentrative export. Before incubation of semi-intact cells at 32°C, gold detected on the surface of the ER (Fig. 10 *A*, *arrowheads*) and nuclear envelope (Fig. 10 *B*, *arrowheads*) was distributed in an apparent random manner throughout the ER cisternal network (Plutner et al., 1992; Balch et al., 1994). The surface density of VSV-G in these ER membranes was 32 ± 6 gold particles per μm^2. In contrast, incubation for 45 min in the presence of cytosol and ATP led to a dramatic change in the distribution of VSV-G, rearranging gold particles to a limited number of VTCs that were well isolated from each other (Fig. 10 *C*). The density of gold over VTCs projected as a flat surface parallel to the ER membrane (referred to as a planar projection) was ~850 ± 250 gold particles per μm^2, a value markedly higher than that observed in the plane of the ER membrane before incubation.

We next used replicas to follow the effects of GTPγS and the Sar1-GTP restricted mutant on budding and concentration of VSV-G. As shown in Fig. 10 (*B* and *C*), incu-

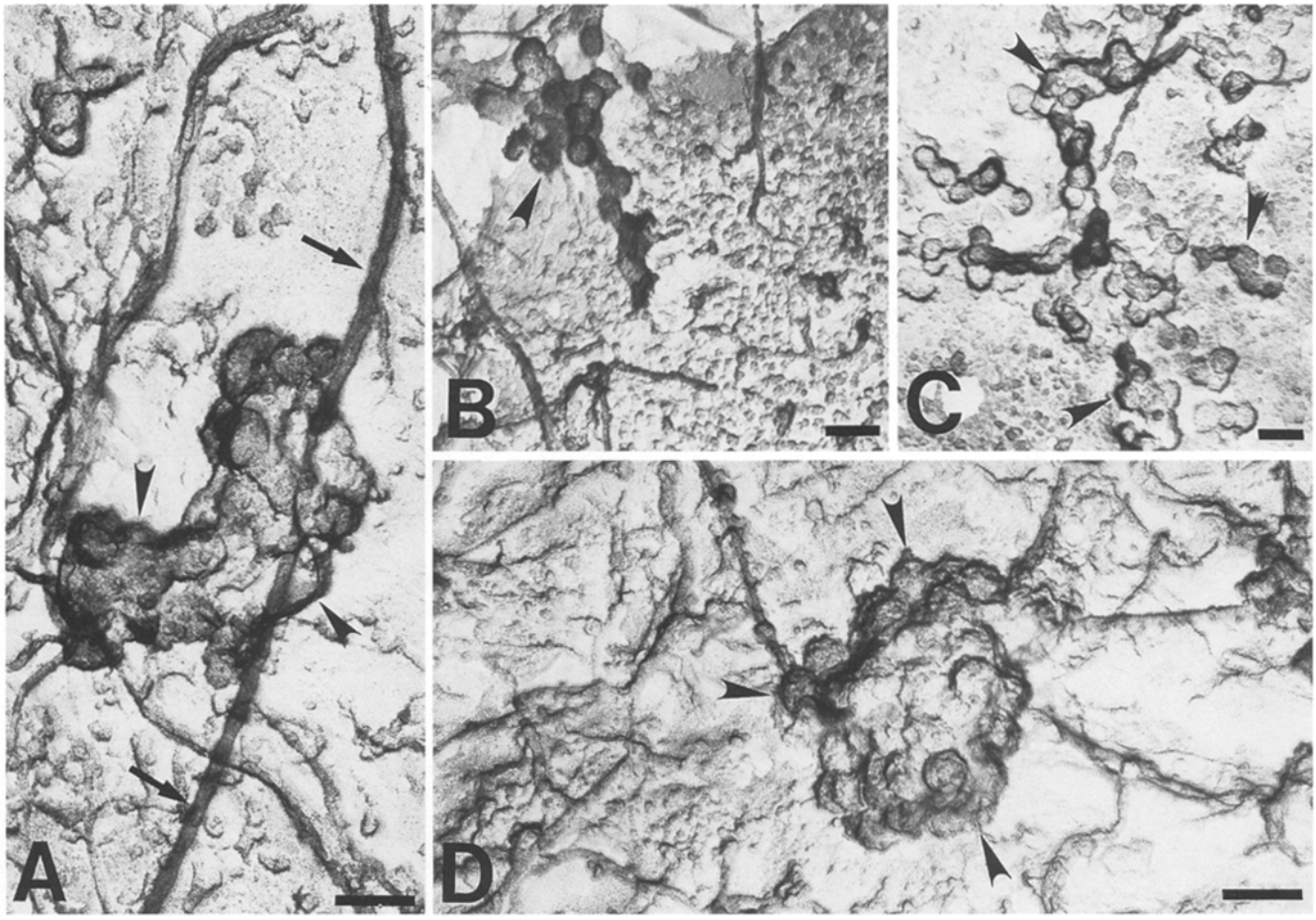

Figure 9. Structure of VTCs adjacent to the ER surface as seen by the quick-freeze, deep-etch replication technique. NRK cells were permeabilized and incubated at 32°C for 45 min in the presence of ATP and cytosol (*A*), or additionally supplemented with 10 μM GTPγS (*B* and *C*) or 1 μM Sar1[H79G] (*D*). Clusters viewed as replicas are present on the ER membrane (*B* and *C*) or the nuclear envelope (*A* and *D*) as indicated by the presence of ribosomes (numerous, small projections on ER surface) (*A–D*) and/or nuclear pores (not shown), respectively. GTPγS accumulated vesicle clusters collapsed onto the surface of the ER during etching usually exhibit a necklace-like morphology with a zig-zag appearance (*B* and *C*). Sar1[H79G] accumulated vesicles appeared as necklace-like structures (not shown) or as compact vesicular clusters (*D*). Note that the cluster in *D* formed in the presence of the Sar1[H79G] mutant has a more vesicular appearance of surface projections than the control cluster shown in *A*, which appears partially tubular in composition. We have noted a frequent association of VTCs with microtubule-like filaments (*arrow* in *A*). Bar, 0.1 μm.

bation of noninfected semi-intact cells in the presence of GTPγS led to the accumulation of vesicles ~80 nm in diameter that, consistent with TEM (Fig. 7, *B* and *C*), had a zig-zag necklace-like appearance when collapsed on the surface of the ER. Immunolabeling of replicas formed in the presence of GTPγS revealed that VSV-G reached a density of 800 ± 200 gold particles per μm^2 in planar projection within clusters. When incubations were carried out in the presence of the Sar1-GTP restricted mutant, necklaces (not shown) and compact vesicular clusters were also observed on replicas (Fig. 9 *D*). In the presence of the Sar1 mutant, VSV-G reached a density of 700 ± 200 gold particles per μm^2 in a planar projection of the cluster (Fig. 10 *E*), reinforcing our previous observations that the budding activity associated with export complexes involves concentration.

Discussion

We have provided the first quantitative, stereological description of the three-dimensional organization of cellular structures involved in transport of cargo from the ER to the Golgi apparatus. Export complexes have a hierarchial organization that can be conceptually divided into three tiers (Fig. 11 *A*). The first tier (Fig. 11 *A*, *dotted box*) consists of closely adjacent buds on a single ER cisterna. Each can give rise to an individual string or group of ER-derived buds containing COPII coats. These budding foci were limited to specific regions of the ER in vivo, suggesting the existence of a defined number of export sites in the living cell. The second tier (Fig. 11 *A*, *cylindrical region outlined by dashed lines*) comes from the observation that buds on one cisterna were often found in close proximity to budding profiles emanating from ER cisternae derived from distantly connected regions of the ER. The third tier of organization encompassing the entire export complex (Fig. 11 *A*, *solid box*) includes ER-derived buds that face into a region housing a central VTC. Tubular elements within VTCs contain distinctive COPI coats and are luminally discontinuous with the ER. While professional secretory

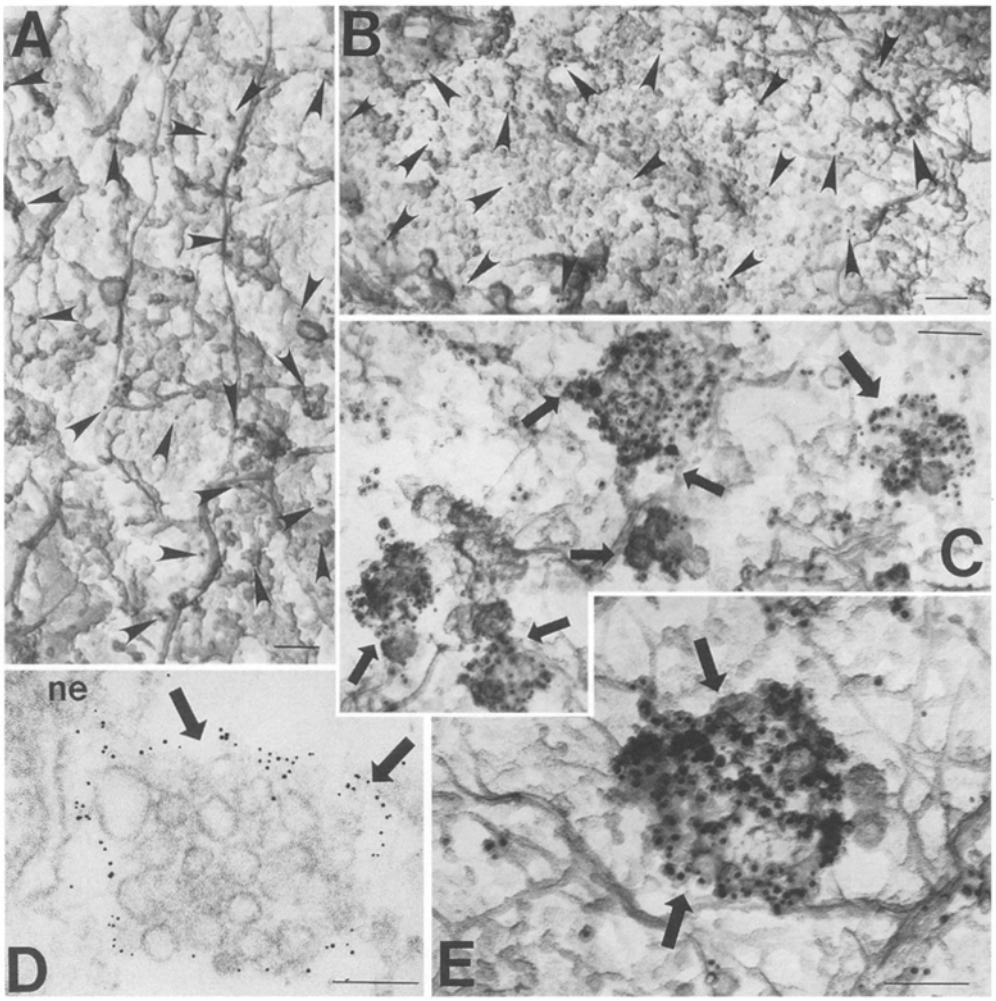

Figure 10. VSV-G is concentrated in ER-derived vesicles and VTCs. NRK cells infected with ts045 VSV at the restrictive temperature (39.5°C) to retain VSV-G in the ER were permeabilized with digitonin (Plutner et al., 1992) and either fixed immediately (*A* and *B*) or incubated for 45 min at the permissive temperature (32°C) in the presence of cytosol and ATP (*C*), or additionally supplemented with 1 μM Sar1[H79G] (*E*). After incubation, cells were fixed and VSV-G labeled with 10 nm (*A–C*, and *E*) or 6 nm (*D*) gold particles using the immunodiffusion protocol as described in the Materials and Methods. Cells were either prepared for thin-section TEM (*D*) or for quick-freeze, deep-etch replication (*A–C*, and *E*). At the restrictive temperature, VSV-G was uniformly distributed within the ER membrane (*A*) or the nuclear envelope (*B*). After a shift to the permissive temperature (*B–E*), VSV-G was concentrated in newly formed 80-nm vesicles associated with export complexes. (*Arrowheads*) Location of 6 nm (*D*) or 10 nm (*A–C*, and *E*) gold particles corresponding to the distribution of VSV-G. Due to the use of an immunodiffusion protocol before preparation of replicas and the high density of label, extended shadows from the gold particles partially obscure membrane outlines. Bar, 0.1 μm.

cells such as those found in the pancreas confine export predominately to a single transitional region juxtaposed to the *cis* face of the Golgi apparatus (Palade, 1975), the two different cell lines used in the present study were found to have export complexes distributed throughout the cytoplasm. Our studies provide evidence that budding from the ER occurs in areas of intense morphological specialization. Each level of organization is discussed in detail below.

Tiers I and II Define the Distribution of ER-budding Profiles

While there is an apparent random distribution of export complexes in the cytoplasm, we found a very high degree of organization in the distribution of ER buds in the cell. We observed not only a high local density on the same stretch of ER membrane (Fig. 11, tier I, *dotted boxes*), but found distantly connected ER bud-bearing zones encircling the same VTC (Fig. 11, tier II, *dashed cylindrical region*), suggestive of a regional specialization of the COPII export machinery. Consistent with this interpretation, buds and vesicles accumulated in semi-intact cells in the presence of GTPγS or the Sar1[H79G] mutant strongly labeled with antibodies specific for mammalian homologues of the yeast components Sec13p and Sec23p.

Both the GTPγS and the GTP-restricted Sar1[H79G] mutant led to the formation in vitro of ER-derived vesicle clusters and strings of vesicles with a necklace-like appearance. Vesicles accumulated as necklaces had no obvious continuity between the lumen of individual vesicles, suggesting that membrane fission had gone to completion. Moreover, in both thin-section and replicas, clusters that formed in the presence of GTPγS or the Sar1 GTP-restricted mutant clearly had a more vesicular surface appearance than those formed in the absence of inhibitors. The fact that separation of vesicles appears to be blocked in the absence of GTP hydrolysis raises the distinct possibly that the function of Sar1 is normally required for this event. Given the fact that uncoating occurs rapidly after budding (Aridor et al., 1995), coat disassembly could be associated with release of vesicles from necklaces.

The morphological effect of GTPγS on the budding from the ER is very different from its effect on Golgi membranes incubated under identical conditions. In the latter case, buds appearing in replicas are isolated, single

structures and are uniformly distributed throughout the entire Golgi surface (Weidman et al., 1993). The regional confinement of budding in ER membranes to necklaces or clusters therefore also supports our interpretation that export occurs from areas of luminal and/or membrane specialization. Since budding from the ER frequently occurs from the tips of short, coated tubules emanating from ER cisternae, clusters and necklaces could be derived from either sequential or synchronous fission of these tubular elements.

In contrast with the fact that export complexes observed in vivo appear to be completely surrounded by budding profiles from topologically distant ER cisternae (Fig. 11 *A*, tier II), semi-intact cells lacked this feature (Fig. 11 *B*). Thus, permeabilization destroys confinement of several sites to one area and allows them to form in a more random fashion. We have previously noted that ER-derived vesicles and downstream compartments are not released from semi-intact cells during incubation in vitro at 32°C (Beckers et al., 1987). In contrast, assays that reconstitute vesicle budding from semi-intact yeast cells (Baker et al., 1988) release free 60-nm COPII-coated vesicular carriers (Barlowe et al., 1994). The inability of mammalian semi-intact cells to release vesicles suggests that vesicles are tethered to a scaffold of unknown composition. In yeast, either vesicles are not linked to such a scaffold, or this aspect has not been successfully reconstituted. In either event, while the striking degree of morphological specialization observed in mammalian cells may contribute to the overall efficiency of budding and transport in the early secretory pathway, it is apparently not essential.

We have previously suggested that export from the ER is accompanied by concentration of VSV-G (Balch et al., 1994). This point was the subject of a recent debate (Balch and Farquhar, 1995; Griffiths et al., 1995*a*). We have now applied an independent approach using quick-freeze, deep-etch methodologies in conjunction with immunolabeling of VSV-G to generate three-dimensional replicas that allow us to directly assess the concentration of VSV-G in ER-derived vesicles. We found, on average, a value of ~800 gold particles per μm^2 in planar projection of clusters accumulated in either the absence or presence of GTPγS, or in the presence of the activated Sar1-GTP restricted mutant. The inclusion of the inhibitors prevents further rounds of vesicle budding, ensuring that we are examining concentration associated with export from the ER. A planar projection, however, is not a good approximation of the total surface area available on clusters for antibody binding. Since only the external surface of vesicles found on the perimeter of clusters is available for antibody binding (Balch et al., 1994; Pind et al., 1994*a*) (see Fig. 11 *D*), a more reasonable estimate of VSV-G density can be determined if we assume that the antibody has access to the outer-half of a shell of 80-nm vesicles that occupy the perimeter of a 0.4-μm sphere (the size of a typical VTC). Compared with the surface area of the planar projection (~0.13 μm^2), the surface area of such a population of vesicles corresponds to a value of ~0.7 μm^2. This is an increase of approximately fivefold over the planar projection. Therefore the actual surface density of VSV-G in clusters observed in replicas is 800 gold particles per μm^2 divided by 5 or 160 gold particles per μm^2. This value, when compared to the average surface density of VSV-G before incubation in vitro (32 gold particles per μm^2), sug-

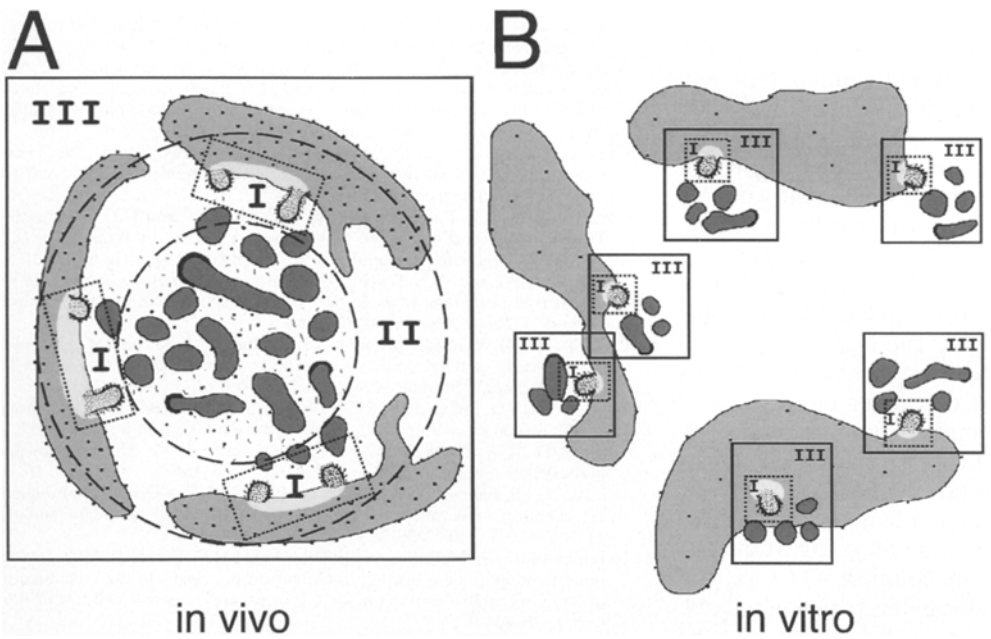

Figure 11. Diagram summarizing the three tiers of organization of ER export complexes in vivo (*A*) and in vitro (*B*). (*A*) An individual ER cisterna contains a collection of closely opposed buds that define a local transitional region (*light zone with buds on the ER*). This specialized region is dominated by the presence of COPII coats and is referred to as tier 1 (*box outlined with dotted line*). Tier II (*cylindrical region outlined by dashed lines*) includes buds on distantly connected ER strands that face a central VTC consisting of a collection of distinct vesicular-tubular elements that have COPI coats. Tier III includes the entire export complex and is outlined by the box with the solid line that encompasses both ER buds and a central VTC. The possible elevated concentration of COPII and COPI coat components within the local cytoplasm of export complexes is depicted by small dots and lines. (*B*) In semi-intact cells, there appears to be a more limited number of ER buds associated with the local transitional region defined by tier I (*box outlined with dotted lines*). The tier II level of organization is completely missing in semi-intact cells, as the association of distantly connected ER strands appears to be lost during cell permeabilization. However, tier III (*box outlined with solid line*) is maintained, highlighting the juxtaposition of VTCs to buds on one ER strand.

gests that VSV-G is concentrated five- to sixfold during budding from the ER. The fold-concentration detected here is very consistent with that observed previously using serial thin-sections (Balch et al., 1994; Pind et al., 1994*a*) or in the present studies in the presence of the Sar1-GTP restricted mutant (Table III). These results confirm the validity of our previous technical advancements (Balch et al., 1994; Balch and Farquhar, 1995) and now firmly establish that cargo is concentrated during ER export (Balch et al., 1994).

The Third Tier: Budding Sites Surround VTCs

A third tier of organization of export sites was found in the striking relationship between flanking ER-connected budding profiles and VTCs to form the functional morphological unit we refer to as export complexes (Fig. 11 *A*, *area enclosed by box with solid line*). Images reconstructed from conventional TEM and those observed in replicas yielded identical results. The distinctive morphological characteristics of the export complexes reconstructed in the present studies are consistent with previous qualitative morphological descriptions (Saraste and Kuismanen, 1984; Schweizer et al., 1988, 1990; Saraste and Svensson, 1991) and a recent study in which a HRP-tagged reporter protein was used to characterize the organization of the ER/Golgi region using immunocytochemistry (Stinchcombe et al., 1995). The replicas were particularly striking in that they allowed us to visualize for first time the overall compact composition of VTCs and their localization to specific foci found on the ER surface.

The overall topological organization of export complexes fits well with the proposed function of the ER in the sorting and concentration of cargo during budding via COPII coats, and the subsequent coupled recycling of proteins from VTCs via COPI coats (Aridor et al., 1995). The close association of these two sorting stations (ER and VTCs) may provide for increased efficiency in ER to Golgi transport and/or promote more rapid exchange of coats within the confines of the complex where a higher local coat concentration may be found. Consistent with this proposal, incubation of pancreatic acinar cells in the absence of ATP (Merisko et al., 1986) or in the presence of brefeldin A (Hendricks et al., 1993; Orci et al., 1993*b*) leads to the accumulation of COPI- and COPII-containing aggregates in transitional regions. The basic morphological organization of export complexes may be more or less extensive in different cell types depending on the relative rates of formation and consumption of vesicles and tubules comprising central VTCs. The extensively fenestrated network found at the *cis* face of the Golgi stack, referred to as the CGN (Mellman and Simon, 1992), is also considered to be a site of membrane recycling. It may be an enlarged variation of the more compact VTCs, reflecting the intensity of vesicular traffic in this region of the cell.

In general, our studies have provided insight into the fundamental morphological organization of the first steps in the secretory pathway that promote the movement of cargo from the ER to the Golgi complex. There has been considerable controversy regarding the morphological organization of this stage of secretory pathway, given the complexity of the pre-Golgi region and the frequent use of reduced temperature to augment the visibility of intermediates (VTCs). Our ability to provide a description of the three-dimensional organization of export complexes at sites distant from the Golgi apparatus under normal incubation conditions now illustrates their basic organization in living cells and their essential role in ER to Golgi transport.

We thank Dr. G. Palade, Dr. M.G. Farquhar, and Michael McCaffery for their many helpful comments concerning the EM.

This work was supported by grants from the National Institutes of Health (GM 42336; CA 586689) (to W.E. Balch), and postdoctoral fellowships from The Human Frontier Science Program Organization, Muscular Dystrophy Association (to T. Rowe), and the Cystic Fibrosis Foundation (to S. Bannykh). This study made extensive use of Core B (Immunoelectron Microscopy) in CA 586689.

Received for publication 22 April 1996 and in revised form 11 June 1996.

References

Aridor, M., S.I. Bannykh, T. Rowe, and W.E. Balch. 1995. Sequential coupling between COPII and COPI vesicle coats in endoplasmic reticulum to Golgi transport. *J. Cell Biol.* 131:875–893.

Baddeley, A.J., H.J.G. Gundersen, and L.M. Cruz-Orive. 1985. Estimation of surface area from vertical sections. *J. Microsc.* 142:259–276.

Baker, D., L. Hicke, M. Rexach, M. Schleyer, and R. Schekman. 1988. Reconstitution of SEC gene product-dependent intercompartmental protein transport. *Cell.* 54:335–344.

Balch, W.E., and M.F. Farquhar. 1995. Beyond bulk flow. *Trends Cell Biol.* 5: 16–19.

Balch, W.E., M.M. Elliott, and D.S. Keller. 1986. ATP-coupled transport of vesicular stomatitis virus G protein between the endoplasmic reticulum and the Golgi. *J. Biol. Chem.* 261:14681–14689.

Balch, W.E., J.M. McCaffery, H. Plutner, and M.G. Farquhar. 1994. Vesicular stomatitis virus glycoprotein is sorted and concentrated during export from the endoplasmic reticulum. *Cell.* 76:841–852.

Barlowe, C. 1995. COPII: a membrane coat that forms endoplasmic reticulum-derived vesicles. *FEBS Lett.* 369:93–96.

Barlowe, C., L. Orci, T. Yeung, M. Hosobuchi, S. Hamamoto, N. Salama, M.F. Rexach, M. Ravazzola, M. Amherdt, and R. Schekman. 1994. COPII: a membrane coat formed by sec proteins that drive vesicle budding from the endoplasmic reticulum. *Cell.* 77:895–907.

Beckers, C.J. M., D.S. Keller, and W.E. Balch. 1987. Semi-intact cells permeable to macromolecules: use in reconstitution of protein transport from the endoplasmic reticulum to the Golgi complex. *Cell.* 50:523–534.

Buccione, R., S. Bannykh, I. Santone, M. Baldassarre, F. Facchiamo, Y. Bozzi, G. Di Tullio, A. Mironov, A. Luini, and M.A. De Matteis. 1996. Regulation of constitutive exocytic transport by membrane receptors: a biochemical and morphological study. *J. Biol. Chem.* 271:3523–3533.

Chavrier, P., R.G. Parton, H.P. Hauri, K. Simons, and M. Zerial. 1990. Localization of low molecular weight GTP binding proteins to exocytic and endocytic compartments. *Cell.* 62:317–329.

Connolly, C.N., C.E. Futter, A. Gibson, C.R. Hopkins, and D.F. Cutler. 1994. Transport into and out of the Golgi complex studied by transfecting cells with cDNAs encoding horseradish peroxidase. *J. Cell Biol.* 127:641–652.

Davidson, H.W., and W.E. Balch. 1993. Differential inhibition of multiple vesicular transport steps between the endoplasmic reticulum and trans-Golgi network. *J. Biol. Chem.* 268:4216–4226.

Griffiths, G., G. Warren, P. Quinn, O. Mathieu-Costelo, and H. Hoppeler. 1984. Density of newly synthesized plasma membrane proteins in intracellular membranes. I. Stereological studies. *J. Cell Biol.* 98:2133–2141.

Griffiths, G., S.D. Fuller, M. Back, M. Hollinshead, S. Pfeiffer, and K. Simons. 1989. The dynamic nature of the Golgi complex. *J. Cell Biol.* 108:277–297.

Griffiths, G., R.W. Doms, T. Mayhew, and J. Lucocq. 1995*a*. The bulk-flow hypothesis: not quite the end. *Trends Cell Biol.* 5:15–18.

Griffiths, G., R. Pepperkok, J. Krijnse-Locker, and T.E. Kreis. 1995*b*. Immunocytochemical localization of β-COP to the ER-Golgi boundary and the TGN. *J. Cell Sci.* 108:2839–2856.

Hendricks, L.C., M. McCaffery, G.E. Palade, and M.G. Farquhar. 1993. Disruption of endoplasmic reticulum to Golgi transport leads to the accumulation of large aggregates containing β-COP in pancreatic acinar cells. *Mol. Biol. Cell.* 4:413–424.

Heuser, J. 1980. Three-dimensional visualization of coated vesicle formation in fibroblasts. *J. Cell Biol.* 84:560–583.

Kreis, T.E. 1986. Microinjected antibodies against the cytoplasmic domain of vesicular stomatitis virus glycoprotein block its transport to the cell surface. *EMBO (Eur. Mol. Biol. Organ.) J.* 5:931–941.

Krijnse-Locker, J., M. Ericsson, P.J.M. Rottier, and G. Griffiths. 1994. Characterization of the budding compartment of mouse hepatitis virus: evidence that transport from the RER to the Golgi complex requires only one vesicular transport step. *J. Cell Biol.* 124:55–70.

Kuge, O., C. Dascher, L. Orci, T. Rowe, M. Amherdt, H. Plutner, M. Ravazzola, G. Tanigawa, J.E. Rothman, and W.E. Balch. 1994. Sar1 promotes vesicle budding from the endoplasmic reticulum but not Golgi compartments. *J. Cell Biol.* 125:51–65.

Lafay, F. 1974. Envelope viruses of vesicular stomatitis virus: effect of temperature-sensitive mutations in complementation groups III and V. *J. Virol.* 14: 1220–1228.

Letourneur, F., E.C. Gaynor, S. Hennecke, C. Demolliere, R. Duden, S.D. Emr, H. Riezman, and P. Cosson. 1995. Coatomer is essential for retrieval of dilysine-tagged proteins to the endoplasmic reticulum. *Cell.* 79:1199–1207.

Lippincott-Schwartz, J. 1993. Bi-directional membrane traffic between the endoplasmic reticulum and Golgi apparatus. *Trends Cell Biol.* 3:81–87.

Lippincott-Schwartz, J., N.B. Cole, A. Marotta, and P.A. Conrad. 1995. Kinesin is the motor for microtubule-mediated Golgi-to-ER membrane traffic. *J. Cell Biol.* 128:293–306.

Lotti, L.V., M.R. Torrisi, M.C. Pascale, and S. Bonatti. 1992. Immunocytochemical analysis of the transfer of vesicular stomatitis virus G glycoprotein from the intermediate compartment to the Golgi complex. *J. Cell Biol.* 118:43–50.

Lucocq, J.M., E.G. Berger, and G. Warren. 1989. Mitotic Golgi fragments in HeLa cells and their role in the reassembly pathway. *J. Cell Biol.* 109:463–474.

Melancon, P., B.S. Glick, V. Malhotra, P.J. Weidman, T. Serafini, M.L. Gleason, L. Orci, and J.E. Rothman. 1987. Involvement of GTP-binding "G" proteins in transport through the Golgi stack. *Cell.* 51:1053–1062.

Mellman, I., and K. Simon. 1992. The Golgi complex: in vitro veritas? *Cell.* 68: 829–840.

Merisko, E.M., M. Fletcher, and G.E. Palade. 1986. The reorganization of the Golgi complex in anoxic pancreatic acinar cells. *Pancreas.* 1:95–109.

Oprins, A., R. Duden, T.E. Kreis, H.J. Geuze, and J.W. Slot. 1993. β-COP localizes mainly to the *cis*-Golgi side in exocrine pancreas. *J. Cell Biol.* 121:49–59.

Orci, L., M. Ravazzola, P. Meda, C. Holcomb, H.-P. Moore, L. Hicke, and R. Schekman. 1991. Mammalian Sec23p homologue is restricted to the endoplasmic reticulum transitional cytoplasm. *Proc. Natl. Acad. Sci. USA.* 88: 8611–8615.

Orci, L., D.J. Palmer, M. Amherdt, and J.E. Rothman. 1993*a*. Coated vesicle assembly in the Golgi requires only coatomer and ARF proteins from the cytosol. *Nature (Lond.).* 364:732–734.

Orci, L., A. Perrelet, M. Ravazzola, F. Wieland, R. Schekman, and J. Rothman. 1993*b*. BFA bodies: a subcompartment of the endoplasmic reticulum. *Proc. Natl. Acad. Sci. USA.* 90:11089–11093.

Palade, G.E. 1975. Intracellular aspects of the process of protein transport. *Science (Wash. DC).* 189:347–354.

Pelham, H.R.B. 1988. Evidence that luminal ER proteins are sorted from secreted proteins in a post-ER compartment. *EMBO (Eur. Mol. Biol. Organ.) J.* 7:913–918.

Pepperkok, R., J. Scheel, H. Horstmann, H.P. Hauri, G. Griffiths, and T.E. Kreis. 1993. β-COP is essential for biosynthetic membrane transport from the endoplasmic reticulum to the Golgi complex in vivo. *Cell.* 74:71–82.

Peter, F., H. Plutner, T. Kreis, and W.E. Balch. 1993. β-COP is essential for transport of protein from the endoplasmic reticulum to the Golgi in vitro. *J. Cell Biol.* 122:1155–1168.

Pind, S., C. Nuoffer, J.M. McCaffery, H. Plutner, H.W. Davidson, M.G. Farquhar, and W.E. Balch. 1994*a*. Rab1 and Ca^{2+} are required for the fusion of carrier vesicles mediating endoplasmic reticulum to Golgi transport. *J. Cell Biol.* 125:239–252.

Pind, S., J.R. Riordan, and D.B. Williams. 1994*b*. Participation of the endoplasmic reticulum chaperone calnexin (p88, IP90) in the biogenesis of the cystic fibrosis transmembrane conductance regulator. *J. Biol. Chem.* 269:12784–12788.

Plutner, H., H.W. Davidson, J. Saraste, and W.E. Balch. 1992. Morphological analysis of protein transport from the endoplasmic reticulum to Golgi membranes in digitonin-permeabilized cells: role of the p58 containing compartment. *J. Cell Biol.* 119:1097–1116.

Rizzolo, L.I., J. Finidori, A. Gonzales, M. Arpin, I.E. Ivanov, M. Adesnic, and D.D. Sabatini. 1985. Biosynthesis and intracellular sorting of growth hormone–viral envelope glycoprotein hybrids. *J. Cell Biol.* 101:1351–1362.

Saraste, J., and E. Kuismanen. 1984. Pre- and post-Golgi vacuoles operate in the transport of Semliki Forest virus membrane glycoproteins to the cell surface. *Cell.* 38:535–549.

Saraste, J., and K. Svensson. 1991. Distribution of the intermediate elements operating in ER to Golgi transport. *J. Cell Sci.* 100:415–430.

Schweizer, A., J.A.M. Fransen, T. Bachi, L. Ginsel, and H.-P. Hauri. 1988. Identification, by a monoclonal antibody, of a 53-kD protein associated with a tubulo-vesicular compartment at the *cis*-side of the Golgi apparatus. *J. Cell Biol.* 107:1643–1653.

Schweizer, A., J.A.M. Fransen, K. Matter, T.E. Kreis, L. Ginsel, and H. Hauri. 1990. Identification of an intermediate compartment involved in protein transport from endoplasmic reticulum to Golgi apparatus. *Euro. J. Cell Biol.* 53:185–196.

Sesso, A., F.P. de Faria, E.S.M. Iwanumra, and H. Correa. 1994. A three-dimensional reconstruction study of the rough ER-Golgi interface in serial thin sections of the pancreatic acinar cell of the rat. *J. Cell Sci.* 107:515–528.

Shaywitz, D.A., L. Orci, M. Ravazzola, A. Swaroop, and C.A. Kaiser. 1995. Human SEC13Rp functions in yeast and is located on transport vesicles budding from the endoplasmic reticulum. *J. Cell Biol.* 128:769–777.

Sterio, D.C. 1984. Estimating number, mean sizes and variations in size of particles in 3-D specimens using disectors. *J. Microsc.* 134:127–136.

Stinchcombe, J.C., H. Nomoto. D.F. Cutler, and C.R. Hopkins. 1995. Anterograde and retrograde traffic between the rough endoplasmic reticulum and the Golgi complex. *J. Cell Biol.* 131:1387–1401.

Tang, B.L., S.H. Low, H.-P. Hauri, and W. Hong. 1995. Segregation of ERGIC53 and the mammalian KDEL receptor upon exit from the 15°C compartment. *Eur. J. Cell Biol.* 68:398–410.

Tooze, J., S. Tooze, and G. Warren. 1984. Replication of coronavirus MHV-A59 in sac cells: determination of the first site of budding of progeny virions. *Eur. J. Cell Biol.* 33:281–293.

Tooze, S.A., J. Tooze, and G. Warren. 1988. Site of addition of *N*-acetyl-galactosamine to the E1 glycoprotein of mouse hepatitis virus-A59. *J. Cell Biol.* 106:1475–1487.

Weibel, E.R. 1979. Stereological Methods. 1. Practical Methods for Biological Morphometry. Academic Press, New York. 415 pp.

Weibel, E.R., and D.M. Gomez. 1962. A principle for counting tissue structures on random sections. *J. Appl. Physiol.* 17:343–348.

Weibel, E.R., and D. Paumgartner. 1978. Integrated stereological and biochemical studies on hepatocytic membranes. II. Correction of section thickness effect on volume and surface density estimates. *J. Cell Biol.* 77:585–597.

Weidman, P., R. Roth, and J. Heuser. 1993. Golgi membrane dynamics imaged by freeze-etch electron microscopy: views of different membrane coatings involved in tubulation versus vesiculation. *Cell.* 75:123–133.

Ziegel, R.F., and A.J. Dalton. 1962. Speculations based on the morphology of the Golgi system in several types of protein secreting cells. *J. Cell Biol.* 15: 45–54.